## ARTICLE

# Femtosecond Laser Induced Breakdown Spectroscopy

Timur. A. Labutin,*[a] Vasily N. Lednev,[b] Alexey A. Ilyin[c] and Andrey M. Popov[a]

The presented review summarizes nearly two decades studies on femtosecond laser induced breakdown spectrometry (fs-LIBS). When ultra-short (<1 ps) laser pulse is used for ablation the physics of laser induced plasma changes dramatically in comparison with ablation by pico- or nanosecond pulses. Femtosecond laser pulse interacts only with electron subsystem while nanosecond pulses continuously interacts with different thermodynamic states of material starting from solid through liquid into plasma. Properties of ultra-short laser radiation, timescale of fs-laser ablation and radiative properties of fs plasma are briefly described. We consider the advantages of fs-LIBS, namely low ablation thresholds, high-spatial resolution, rapid analysis of samples, which require minimal invasion, high-efficiency transportation of laser radiation under filamentation mode for remote analysis. Also we discussed possible limitations of the technique and different approaches to overcome such constraints keeping unique possibilities of fs-LIBS.

## 1 Introduction

Pulsed solid state Nd:YAG laser with nanosecond pulse duration is a typical "work horse" for laser-induced breakdown spectrometry setup. A perspective tool became available for novel LIBS applications with development of a new generation of ultra-short laser systems with femtosecond pulse duration in late 1980-s. Femtosecond laser induced breakdown spectrometry (fs-LIBS) can improve figures of merit for LIBS quantitative analysis (better reproducibility, absence of fractional evaporation, small damage, *etc*.) due to changes in laser-matter interaction.

Fs-LIBS makes a long "journey" of more than 25 years from first ultrashort pulses generation to elemental analysis. First generation of femtoseconds laser pulses was demonstrated in 1970-s[1] and invention of Ti:Sapphire laser in 1980-s stimulated the growing attention to femtosecond systems.[2] Invention of chirped-pulsed amplification technique in 1985 was a revolutionary breakthrough in femtosecond laser systems resulting in appearance of a powerful femtosecond laser pulses.[3] First plasma spectroscopy studies induced by femtosecond pulses (700 fs) were carries out four years later and were mainly focused on plasma physics problems.[4] The rapid growth of publications on femtosecond laser plasma was started when commercial powerful laser system became available. The first emission spectrum of femtosecond laser plasma was ascribed only in 1998 to control laser machining.[5] The first application of femtosecond pulses to analytical chemistry problems was demonstrated only in 2000 by Margetic *et al.*[6] Seven years later Gurevich and Hergenröder[7] have presented a first review on achievements and future perspectives of fs-LIBS. After this review a numerous papers on fs-LIBS have been published in literature. In current review we summarized the state-of-the-art in studies of femtosecond ablation and plasma physics, instrumentation and applications.

Ultrashort pulse duration gave numerous benefits for the fs-LIBS: low ablation threshold, absence of fractionation vaporization, improved spatial resolution for 3D mapping applications, small ablated mass, sample damage, *etc*. All these benefits are originated from physics of femtosecond ablation and plasma which is described in Section 2. In Section 3 we summarize analytical performance of fs-LIBS and discuss its perspective. The possibility of high-efficiency transportation of laser radiation under filamentation mode for remote analysis and applications of filaments in LIBS, which is also called Filament-Induced Breakdown spectroscopy (FIBS), are discussed in Section 4. A special attention is given for the comparison of analytical figures of merit (sensitivity, accuracy, precision) as well as unique applications (filament induced breakdown spectroscopy).

## 2 Fundamentals of femtosecond laser-induced plasmas

### 2.1 Properties of ultra-short laser radiation and typical equipment

Femtosecond pulse generation is based on Kerr lensing in the gain medium[8,9] and a Ti:Sapphire crystal is a commonly used for this purpose. In contrast to nanosecond laser (Q-switched),

[a.] Department of Chemistry, Lomonosov Moscow State University, Leninskie Gory, 1-3, 119991, Moscow, Russia, e-mail: timurla@laser.chem.msu.ru
[b.] National University of Science and Technology "MISiS", Leninskiy Prospect, 2, 119049, Moscow, Russia, e-mail: vasilylednev@gmail.com
[c.] Far Eastern Federal University, Sukhanova Street, 8, 690950; Institute of Automation and Control Processes of FEB RAS, Radio Street, 5, 690041, Vladivostok, Russia, e-mail: kunashir@gmail.com
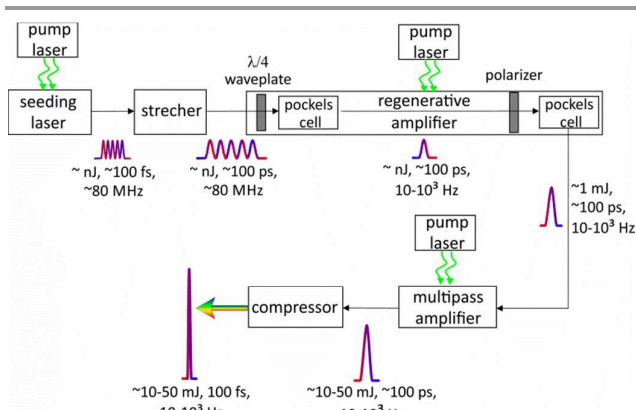
Fig. 1. Typical scheme of femtosecond laser system. Pulse repetition rate is reduced to 1-10 Hz for systems with pulse energy exceeding 10 mJ.

output energy of femtosecond oscillators (~ 1 nJ) is clearly insufficient to exceed a threshold for plasma generation. Therefore, femtosecond laser for LIBS is supposed to use one or more additional amplifiers to a seeding laser, as shown in Fig. 1. Normally, the seeding laser produces a train of femtosecond pulses with a central wavelength near 800 nm and repetition rate ~80 MHz. Femtosecond pulse can be broadened due to a self-phase modulation in the media with a nonlinear refractive index and group velocity dispersion (GVD) by optical elements of the laser. Pulse duration of the seeding laser can be tuned by modifying GVD of the cavity which is determined as follows:

$$GVD = \frac{d}{d\omega}\left[\frac{1}{v_g}\right], v_g = \left[\frac{dk(\omega)}{d\omega}\right]^{-1},$$

where $k(\omega)$ is wave vector and $v_g$ is group velocity. One can easily see that the group velocity is different for various wavelengths. The influence of dispersion properties of a material on instantaneous frequency of femtosecond pulse is characterized by a chirp. The pulse is said to be positively "chirped" when the instantaneous frequency is red-shifted in a pulse front and blue-shifted in a trail as shown in Fig. 2.
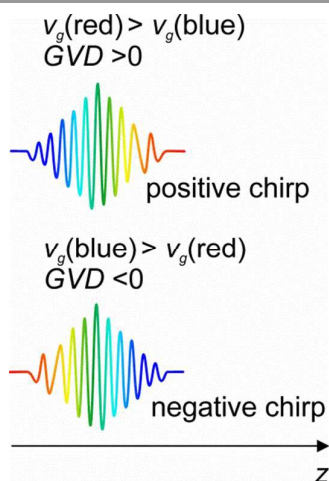


Fig. 2. Chirp and GVD.

Positive chirp of intracavity elements can be compensated by the media with negative GVD like grating or prism pairs to obtain short output pulses.

To avoid the damage of Ti:Sapphire crystal it is essential to keep the power density in the amplifier below the Ti:Sapphire damage threshold. This can be achieved by using the chirped pulse amplification technique, which is supposed to incorporate into a stretcher reducing power and broadening pulses, before the regenerative amplifier with consequent narrowing of pulses with a compressor after amplification. Usually stretcher and compressor represent a pair of gratings or prisms. Pulse repetition rate is reduced to $10\text{-}10^3$ Hz by Pockels cells to provide maximal amplification without overheating of gain medium in a regenerative amplifier. Thus, the pulse energy increases from several nJ to roughly mJ level. The amplification in multipass amplifier is limited by the number of passes (usually 2-8) due to difficulties of focusing into a single Ti:Sapphire rod. Finally, a pulse is usually compressed down to duration of 30-500 fs, although sub-4-fs pulses can be obtained in specially designed laser systems.[10,11] Femtosecond pulses are also broadened by optical components of LIBS system. The output pulse duration for Gaussian transform-limited pulse is determined as:[9]

$$\tau = \tau_0\sqrt{1 + \left[\frac{4\times\ln 2\times(GVD\times L)}{\tau_0^2}\right]^2},$$

where $\tau_0$ is incoming pulse duration, $L$ is a length of the dispersive material. For example, initially unchirped 30-fs pulse at 800 nm becomes broadened to 40 fs after 6 mm-thick focusing BK-7 lens ($GVD$ = 44.6 fs²/mm at 800 nm).

The temporal profile of the femtosecond laser pulse and the intensities of pulse components are of key importance in laser-target interaction. During generation, amplification, spectral and temporal shaping, a number of physical processes affect the temporal shape of the pulse. Final pulse may consist of pre-pulses, post-pulses and main pulse on top of a very broad pedestal (see Fig. 3).[12,13] This nanosecond pedestal, or an amplified spontaneous emission (ASE), corresponds to noise photons amplifying in the same way as the main pulse. ASE duration does not exceed 10 ns and may contain up to 25% of the total pulse energy[14] with the ratio of the peak intensity of the main pulse to the peak intensity of ASE ~ $10^5$-
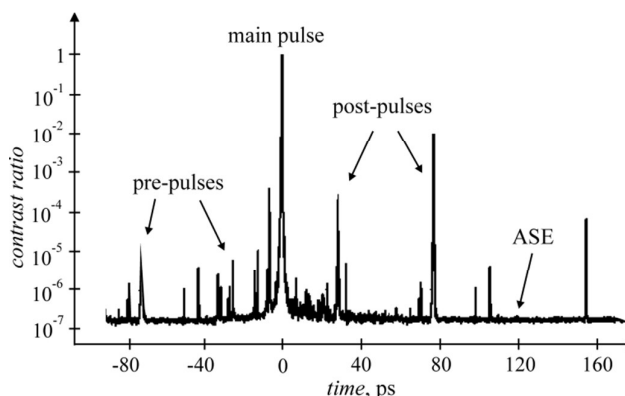


Fig. 3. Temporal profile of fs laser pulse with ASE, pre- and post-pulses obtained by 3rd order cross-correlator.

$10^8$ (contrast ratio).[12,13] Pre- and post-pulses are caused by Fresnel reflections in optical elements[12,13] and radiation leakage out of regenerative amplifier on each pass of a beam in a cavity.[7] Their durations are greater than or equal to the main pulse, and contrast ratio varies in wide range from $10^2$ to $10^8$ depending on a laser system. Pre-pulses can create plasma before arrival of a main pulse that leads to reducing the main pulse energy deposition in an analyzed sample.[13] Saturable absorbers, frequency doubling and additional Pockels cells can be used to correct temporal shape and improve contrast ratio. Usually pulse duration and temporal shape are controlled by fast photodiodes, streak cameras auto- and cross-correlation methods.[9]

### 2.2 Filamentation

Visually, the laser-induced filament in air represents the long thread luminous due to emission of first negative system of $N_2^+$ $B\ ^2\Sigma_u^+ \longrightarrow X\ ^2\Sigma_g^+$ and second positive system of $N_2$ $C\ ^3\Pi_u \longrightarrow B\ ^3\Pi_g$. A filament can appear at high peak laser intensity. The theoretical estimation was carried out by Chiao et al.[15] in 1964. Although, the first filament was induced in liquids by powerful nanosecond pulses in 1965,[16] it was observed in air only in 1995 when powerful femtosecond laser systems with needed peak power of several GW became available.[17] Therefore, filamentation in the atmosphere is a subject to intensive investigations over a period of past two decades. Generally, these investigations are related to the self-focusing of laser beam, conical emission, supercontinuum generation, etc.[18-20] The detailed description on filament physics and applications can be found in several reviews.[21-24]

Filamentation arises due to strong spatiotemporal self-modulation of femtosecond pulses, i.e. the self-focusing initiates plasma that defocuses the propagating laser beam. The series of self-focuses from front part of the pulse give rise to the luminous plasma channel or so-called filament. The back part of the pulse experiences self-phase modulation and self-stepping resulting in a strong spectral broadening (supercontinuum). On average, filamentation area has 50-200 μm diameter, its length varies depending on pulse power, medium and laser wavelength.[23,25] Continuous filament was observed with length of ~100 m[26] and recently up to 1 km.[27] It should be noted that tuning of pulse chirping allows precise control of filament initiation at desired distances up to 20 km.[28]

For the laser radiation the power of which exceeds essentially a self-focusing threshold in the air (1.7–10 GW for λ = 800 nm),[29-31] many filaments emerge by reasons of non-homogeneity of intensity distribution in the cross-section of the laser beam[21,22] and (pre-)post-pulses filamentation.[32] For weakly focused laser beams, intensity clamping is observed as a consequence of balance between the Kerr-type self-focusing and plasma induced defocusing. In air filament, intensity does not exceed threshold value of ~$5 \cdot 10^{13}$ W/cm$^2$ even with an increase of femtosecond pulse energy.[23,33] This situation corresponds to low-NA (Numerical Aperture < (3-5)$\cdot 10^{-3}$) or nonlinear focusing regime in filamentation.[34] In case of high-NA or linear focusing regime, geometrical focusing and plasma

defocusing are the primary contributors to the filamentation process, while Kerr-type self-focusing plays secondary role. Intensity exceeds threshold value of $5 \cdot 10^{13}$ W/cm$^2$ in this case.[33,35] Xu et al.[33] suggested simple formula for estimation of the intensity of the laser radiation in the filament:

$$I = 79 \times \left( \frac{2.6}{R} - 1 \right)^{-0.34} \times 10^{12}\ \text{W/cm}^2$$

where $R$ is intensity ratio (391.2 nm/337 nm) of nitrogen molecule lines.

Electron density in plasma filaments varies from $10^{14}$ to $10^{18}$ cm$^{-3}$ depending on the experimental conditions.[29,36-38] Basically, electrons are appeared due to multiphoton ionization (MPI), its ionization rate is proportional to $I^K$, where $K$ is the number of absorbed photons necessary to ionize molecules. Ionization potentials of air molecules are 15.6 eV ($N_2$) and 12.1 eV ($O_2$). Therefore, $K(O_2) = 8$ and $K(N_2) = 11$ for λ = 800 nm (photon energy is 1.55 eV). Kasparian et al.[39] have shown that $K(O_2) \approx 6.5$ and $K(N_2) \approx 7.5$ for intensities $I < 10^{14}$ W/cm$^2$ that indicate the occurrence of tunnel ionization (TI). In other words at such intensities electron in molecule pass through the potential barrier and escape from the molecule. For plasma induced by ns pulses, electron avalanche ionization is characteristic. Seed electrons starting avalanche arise due to MPI of impurities with low ionization potential.[40] Then the energy of electrons is increased by inverse Bremsstrahlung effect, i.e. electrons absorb photon in the field of ions or atoms (molecule). This process needs approximately 350 fs in air.[41] Hence, electron avalanche ionization can also take place in filaments induced by laser pulses with duration exceeding this value. For $I < 2 \cdot 10^{14}$ W/cm$^2$, photoelectrons ejected from molecules have initial kinetic energy of a few eV, which corresponds to an initial free-electron temperature ~ $10^4$–$10^5$ K.[42,43] These values are much smaller than 60 eV, i.e. initial temperature of plasma induced by ns pulse with $I = 2 \cdot 10^{11}$ W/cm$^2$.[44] That is why electron density in filaments less than that of nanosecond plasma which can reach critical values of $1.7 \cdot 10^{21}$ cm$^{-3}$ (at λ = 800 nm). It is interesting to note that velocity of filament expansion is $2 \cdot 10^8$ m/s,[32] which is close to speed of light. In the case of ns pulse, plasma expanding due to single photon UV and avalanche ionization has velocity ~ $10^5$ m/s.[45]

In contrast to extensive studies of self-focusing, harmonics and supercontinuum generation etc., molecular and atomic emission of plasma generated by laser filamentation is less investigated. Temporal characteristics of atom and molecule emission of laser plasma filaments can be found in Refs.21,46-48 Application of laser filamentation for spectrochemical analysis will be considered in Section 4.

### 2.3 Interaction of femtosecond pulses with condensed matter

Negligible heat transfer from the irradiated area and absence of plasma-laser interactions are the main features of femtosecond laser ablation with the comparison of nanosecond one. Therefore, absorbed laser energy is localized in relatively small (even less than μm for near-field focusing[49]) region with simply controlled dimensions.[50,51] Also absorption

wave moving towards laser beam is absent in femtosecond plasma.

Interaction of femtosecond pulse with matter involves many physical phenomena, such as light absorption, non-linear ionization, plasma formation, thermal conduction, ablation, *etc.* Comprehensive review of these phenomena can be found in recently published works.[52,53] As regards to LIBS, plasma and ablation dynamics are very important. Firstly, let's consider early stage of plasma evolution. Free electrons in a metal absorb laser photons via the inverse Bremsstrahlung process at the very beginning of irradiation and do not obey Fermi–Dirac distribution in the absorption region of laser radiation (~ 10 nm depth). The non-thermalized ballistic electrons transfer absorbed laser energy to deeper sample layers (~ 100 nm).[54] A few femtoseconds is required to establish thermal equilibrium through electron–electron collisions in electron subsystem.[53] Hot electrons overcome the potential barrier[52] and are emitted from the surface. Meanwhile, another part of electrons, photo-induced electrons, overcome the barrier due to multiphoton absorption, since barrier energy exceeds photon energy at $\lambda = 800$ nm for most materials. At this time period, ions of lattice are cold because electron-lattice thermalization occurs on picosecond time scale. Electrons emitted from the surface create electrostatic field, which pulls ions out of the surface. Fast ion ejection is called as double layer effect[55] or electrostatic ion removal.[52] It was shown that approximately several tens of femtoseconds is necessary to remove ions.[52] After free electrons and ions are generated, electrons can increase their energy due to "parachute effect"[56] and impact ionization is also started.[57]

Another mechanism of plasma formation is realized for dielectrics and semiconductors since an additional energy is needed to create the free carriers in a conduction band. Absorption of one or two photons is enough for electron transition from valence band to conduction one due to relatively narrow bandgap. When electron density reaches value ~ $10^{18}$-$10^{19}$ cm$^{-3}$, electron avalanche is launched. At this stage, electrons absorb energy via inverse Bremsstrahlung, and avalanche ionization prevails over other ionization mechanisms.[53] Seed electrons in the conduction band are generated by MPI in dielectrics. As soon as definite density of these electrons is achieved, avalanche ionization is initiated. In the case of high laser intensities, TI also takes place in superficial layer of sample.[53,58] Another mechanism of plasma formation typically observed for dielectrics is Coulomb explosion (CE). Emission of electrons from surface leads to accumulation of an excessive positive charge in superficial layer of sample. For strong field, electrostatic repulsive forces between ions disintegrate layer (several nanometers depth) resulting in CE during first hundreds of femtoseconds.[53] Coulomb explosion was observed at extreme intensities of ~ $10^{19}$ W/cm$^2$ for metals,[58] whereas it is still debated for semiconductors at high intensities ($I \geq 10^{14}$ W/cm$^2$).[53]

In ambient conditions, gas layer in vicinity of sample can be ionized by laser radiation and/or high-energy free electrons ejected from sample. It should be noted that front part of the laser beam reflected from the sample can interfere with the

trail of the beam resulting in laser intensity increase by a factor of $\left(1 + \sqrt{R}\right)^2$ above the surface with reflectivity $R$.[59] Free electrons of gas and electrons removed from the sample can become seed electrons for avalanche ionization,[60] which can be supported by post-pulses.

Early stage of plasma evolution was investigated both experimentally and theoretically in Refs.60-62. In case of vacuum ($4\cdot10^{13}$ W/cm$^2$, 50 fs, 800 nm), electron cloud above the surface of Cu is split into fast-moving (~$10^7$ m/s) and slow-moving (~$10^4$ m/s) parts, and this can be explained by repulsive electric field generated within the electron cloud. Electron density in fast-moving cloud decreases from ~$10^{20}$ to ~$10^{17}$-$10^{16}$ cm$^{-3}$ during first 4-12 ps. In case of ambient gas, target plasma with air breakdown is observed (100 fs, ~$4\cdot10^{14}$ W/cm$^2$, 800 nm). For target plasma formation, simulation reveals existence of double layers (electrons and ions) with maximal electronic density of $10^{20}$ cm$^{-3}$. Electron front in air breakdown area moves faster than electrons near the target surface due to attraction of lesser quantity of ions. Air molecules ionized primarily due to MPI with consequent electron avalanche, while impact ionization by target electrons plays secondary role. Electron density is about $10^{20}$ cm$^{-3}$ near the target and $10^{19}$ cm$^{-3}$ in electron front. Zhao and Shin[62] claim that emission of Si$^+$ and Si$^{2+}$ ions is observed from several tens to 150 fs due to CE, whereas electrostatic ion removal and thermal ejection are characteristic for Cu$^+$ and Cu$^{2+}$ ions. It should be noted that air breakdown threshold by femtosecond pulses is ~ (2-4)$\cdot10^{14}$ W/cm$^2$ at $\lambda = 800$ nm.[63-65] The above mentioned mechanisms of plasma formation can be treated as non-thermal mechanisms, which launch ablation on femtosecond time scale. Brief description of laser-matter interactions related to thermal and mechanical effects will be given below. These processes are occurred on picosecond time scale and resulted in larger amount of ejected material.

Laser-matter interaction at femtosecond scale is usually described by two-temperature model,[66] when electrons and lattice are characterized by different temperatures. Electrons transfer absorbed laser energy to initially cold lattice through electron-phonon interaction that leads to electron-lattice thermalization during a few picoseconds.[67-69] Temperature of lattice grows also after laser pulse resulting in melting of irradiated layer. Heating up to melting temperature takes tens of picoseconds.[70,71] Melting depth reaches hundreds of nanometers and depends on laser fluence and material. It should be stressed that ultrafast melting is observed for semiconductors on time scale of ~ 100 fs at intensities of ~ $10^{12}$ W/cm$^2$.[68] Transfer of ~10-15% valence electrons to conduction band leads to lattice instability and disordering.[72] Since ultrafast disordering occurs at temperatures below melting point, it is also called non-thermal or cold melting. High temperature of superficial layers (tens nanometers in depth) up to $3\cdot10^4$ K can lead to direct evaporation to gas phase with phase trajectory lying above critical point (supercritical regime or atomization).[67,73] Critical point phase separation is observed at temperatures close to critical point. In this case, phase trajectory of sample layer crosses liquid branch of binodal and enters into the region of metastable

liquid.[67,74] Lifetime of this state is only several picoseconds, and substance instantaneously disintegrates into gas-liquid mixture.[67,74,75]

Tensile stress caused by thermoelastic and shock waves leads to formation of voids at certain depth. Some of the voids are coalesced resulting in mechanical layer decomposition and spallation at tens of picosecond.[70,76] This mechanism arises if metastable liquid state exists longer than the mechanical fractures at temperatures below critical point. Otherwise, phase explosion occurs with disintegration of matter into gas and droplets.[74,75] This mechanism is similar to the critical point phase separation, but unlike of it phase explosion is observed at lower temperatures. Although ~80% ablated mass of metals at irradiance ~ $10^{13}$-$10^{14}$ W/cm$^2$ is ejected by mechanical decomposition,[67,74] this mechanism can be suppressed by recoil pressure of the vapour/cluster plume at high laser fluences.[53] Finally, plasma expansion and intensive ejection of vapor and droplets lead to shock wave formation in surrounding gas.[69,77] Summarizing our considerations, main processes of plasma formation and ablation at laser intensities of ~ $10^{13}$-$10^{15}$ W/cm$^2$ are shown in Fig.4.

The competing processes lead to formation of several fractions in plasma plume. Three different velocity populations can be discriminated during the plasma expansion. Coulomb explosion firstly produces ions with high kinetic energy, which are followed by neutrals formed by adiabatic expansion with a velocity comparable to the nanosecond regime, and lastly by nanoscale clusters.[78] These nanoparticles produce broadband continuum radiation in plasma similar to black body emission from a macroscopic object.[79] Moreover, different ablation mechanisms for various types of solids lead to a strong variation of the fractional composition of ejected matter and nanoparticles. In papers of Noël *et al.*[80] and Axente *et al.*[81] plasma composition was considered during femtosecond ablation of copper and fused silica, respectively. A ''slow'' component of high intensity is located close to the target, whereas a ''fast'' component of lower emission intensity is observed at larger distance. It was shown with the use of fast imaging and optical emission spectroscopy that two clouds of
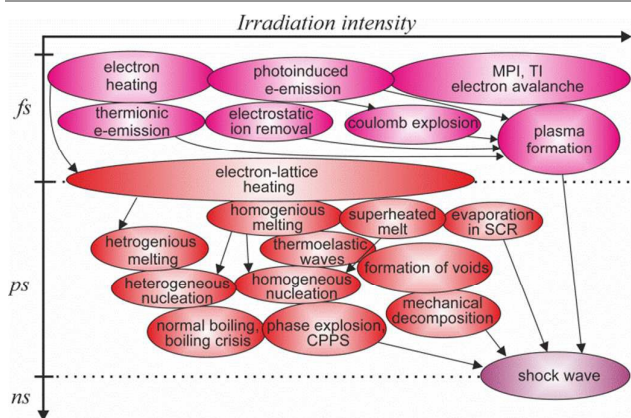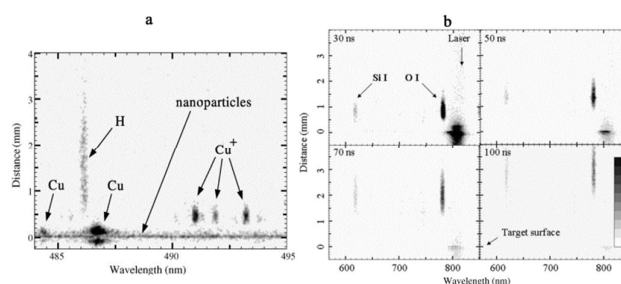


Fig. 5. Plume emission intensity vs. distance and wavelength: a) recorded 20 ns after the laser pulse for ablation of copper with fluence 4 J cm$^{-2}$ (reproduced from Noël *et al.*[80] with the permission of Elsevier Science), b) fused silica for different delay times between the laser pulse and the observation gate (reproduced from Axente *et al.*[81] with the permission of IOP Publishing)

nanoparticles were generated during femtosecond laser ablation in vacuum ($10^{-4}$ Pa): fast frontal plume component mainly consisted of small clusters (''fast'' component) and larger particles were located mostly at the back (''slow'' component). Spectra registered during metal ablation revealed that emission from the ''fast'' component consisted of mainly spectral lines of neutral atoms and ions whereas a blackbody-like continuum dominates the emission of the ''slow'' component (Fig. 5a). Unlike metal ablation, the plasma generated by femtosecond laser on a fused silica target had only ''fast'' component (Fig. 5b). The characteristic expansion velocity of this unique component was about one order of magnitude higher than of ''fast'' component in case of metals.

Since sufficient part of pulse energy presents ASE, it can influence ablation process.[14,69,82] It was shown that ASE can create a relatively thick melt layer on a surface before main pulse with increasing ejected volume of material. Schematic view of femtosecond ablation with ASE is shown in Fig. 6 (time $\tau = 0$ corresponds to main pulse with duration $t_p$).[69] Sample surface is heated (Fig. 6a) and can be melted by pre-pulse or ASE before main pulse. Main pulse interaction leads to hot plasma formation with emission of electrons and breakdown in ambient gas (Fig. 6b). After electron and lattice temperatures become close to each other at $\tau \approx \tau_{eq}$, different layers of material can be evaporated, melted or being in plasma or metastable state. Then homogeneous nucleation occurs in superheated melt (Fig. 6d). Some delay in phase explosion or mechanical decomposition can be explained by boiling crisis (Fig. 6e),[69] observed earlier for ablation by nanosecond pulses because of a formation of a continuous vapor layer or film over the liquid melt.[83,84] Phase explosion starts at $\tau = 700$ ps - 1 ns, when pressure decreases due to vapor expansion. Shock wave can be detected up to $\tau \approx 100$ ns (Fig. 6f). Vapor and sub-micrometer particles are ejected up to 500-700 ns (Fig. 6g). Sometimes continuous liquid jets or melt droplets of several micrometer size is observed up to $\tau \approx 1$ µs.

Thus, the features of femtosecond pulses are duration less than thermalization in any medium, chirping and controlled filamentation which permits laser energy transfer over a long distance in atmosphere. At the same time, mechanism of ablation and plasma formation strongly depends on material,



Fig. 4. Sketch of main physical phenomena leading to plasma formation and ablation. CPPS is critical point phase separation, SCR means supercritical regime.
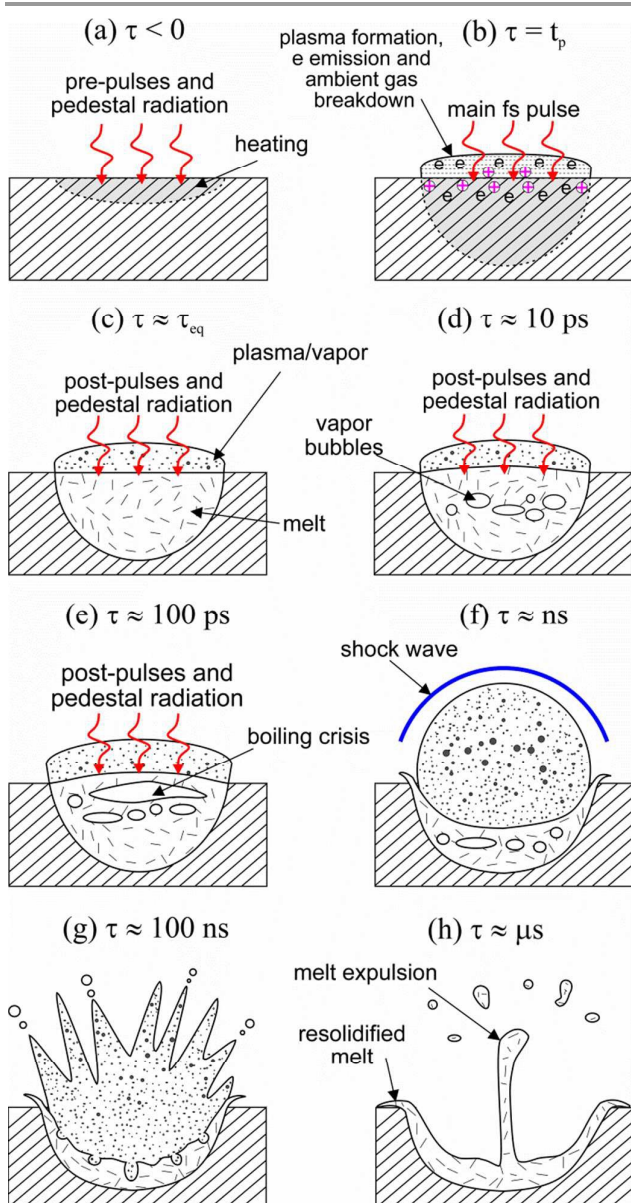
Fig. 6. Schematic view of plasma formation and ablation. $t_p$ is a duration of main fs pulse, $\tau_{eq}$ is a characteristic time of the equilibrium establishment between electrons and lattice.

laser fluence, wavelength, pulse duration, layer depth. In contrast to nanosecond pulses, there is no shielding effect and absorption wave of laser radiation in ambient gas resulting smaller initial temperature and electron density and, as a result, the reduced continuum radiation. In combination with smaller ablation thresholds, this leads to considerable ejection of material on picosecond time scale. Minimal heat-affected zone, sputtering and mechanical deformations can provide high depth/spatial resolution and precise machining due to negligible heat transfer from energy absorption area.

## 3 Analytical performance of femtosecond LIBS

### 3.1. Depth profiling

An unique feature of femtosecond laser ablation is a small amount of melting in comparison with ablation produced by nanosecond pulses. As a result, the craters produced by fs laser have more even walls without the clear rims than ones produced by ns lasers,[85] and the structure, diameter and depth of craters are well reproduced. Lopez-Claros *et al.*[86] have recently studied the thresholds for single-shot femtosecond ablation of different metals (Pb, Ag, Zn, Sn, Cr, Cu, W, Ni and Fe). The craters exhibited similar size (~40 μm at 4-9 J/cm²) and shape regardless of the sample type, energy range (for energies per pulse <400 μJ) and accumulated energy dosage (<500 laser shots on the same sample position). Such a peculiarity allows the use of fs-LIBS to accurately construct in-depth profiles of metallic alloys. Since the goal of a quantitative in-depth analysis is to obtain the local concentration of an analyte as a function of the layer depth with respect to a distance perpendicular to the solid surface,[87] analysts have to solve two tasks. It is essentially important to find a conversion function of the dependence of LIBS intensity on pulse number, *i.e.* "measured profile", into a content-depth relation, *i.e.* "true" depth profile. Another obstacle for in-depth measurements by LIBS is accuracy validation by means of independent methods, desirable non-destructive techniques because of removing material from a surface. To quantitatively describe an ability of technique to distinguish the local content between two levels of depth profile, the term of *depth resolution* is used. According to IUPAC terminology, it is "the distance between the 84 and 16 percent level of the depth profile of an element in a perfect sandwich sample with an infinitesimally small overlap of the compounds."[88]

General practice to estimate depth resolution for techniques with laser ablation is to calculate the average value of ablation rate from pulse-to-pulse measurements of crater deepening by several profilometry techniques in terms of μm/pulse or nm/pulse.[89] In an ideal case, it should be permanent and crater is linearly deepened under the fixed fluence. An ablation depth per pulse, $l_{abl}$, for ultrafast laser processing of metallic alloys can be estimated by inequality:[52]

$$\frac{l_s}{2}\ln\left(\frac{F_{abl}}{F_{thr}}\right) + l_{mono} < l_{abl} < \frac{F_{abl}-F_{thr}}{n(\varepsilon_b+\varepsilon_{esc})} + l_{mono},$$

where $F_{abl}$ and $F_{thr}$ are ablation and threshold fluences, respectively, the depth of the only one surface atomic layer, $l_{mono}$, can be estimated as $\sim n_a^{-1/3}$, $l_s$ is the depth of thin layer in which energy of fs pulse is absorbed, and, finally, $\varepsilon_b$ and $\varepsilon_{esc}$ are the energy spent on breaking bonds and kinetic energy of ablated atoms, respectively. It is obvious that the lower the ablation fluence is used, the shallower crater will be. This means that distribution of energy across a beam defines ablation rate; because of this, a beam profile influences on crater shape, its diameter and depth. By using a Gaussian beam, the crater shape becomes cone-like that applied to make, for example, grooves with the regular shape.[90] In such a way, a Gaussian beam can be considered as a 'knife' produced deeper craters. On the other hand, flat-top beam profile is capable for production of straight-wall craters with flat

bottom.[91] For example, Banerjee *et al.*[92] have recently demonstrated that the ablation rates for Gaussian and flat-top beams were differed in 30 times (1 μm/pulse *vs.* 30 nm/pulse, respectively) as like as a ratio of laser fluences of the beams, 42 J/cm² *vs.* 1.4 J/cm². Like an 'awl', a Gaussian beam has quickly (<30 shots) drilled the upper thick layer of silicon (32 μm) to reach to the buried layers of Cu and Cr (about several μm). Only two or three pulses of this laser were inside the thin layers of copper and chromium. Unlike Gaussian beam, flat-top beam allowed the improvement of depth resolution down to 30 nm with prolongation of ablation up to 1200 pulses.

Another possibility to deeply penetrate into a sample provides with non-diffracting Bessel beams. They have the intensity distribution across a beam described by Bessel function of *n*th-order $J_n$:[93] the beam shape has a central core with a series of concentric rings. An unique feature of such kind of beams is that the intensity profile of its central core propagates without experiencing appreciable spreading. A circular slit[94] or a conical-shaped axicon[95] are usual tools to generate Bessel beams. The most spectacular demonstration of the ability of Bessel beams is drilling $\lambda/4$=200 nm channels with aspect ratio ~100 by a single shot of 650 nJ 230 fs pulse in glass.[96] The robustness of Bessel beams to the presence of obstacles and self-healing ability makes them very attractive for laser processing of dielectrics with powerful femtosecond pulses. Since there were, to our best knowledge, no works on the use of LIBS technique for spectral monitoring ablation process with Bessel beams of zeroth or first orders, we suggest this field of LIBS applications is very prospective, especially, in micromachining and material processing.

Generally, LIBS is applied to measurement of the thickness of coatings,[97] layers, *etc.* as an auxiliary tool which is needed to detect a transition between two different layers. In this case, to decide that the crater bottom crossed the interface between two layers, analysts should observe sharp change in the pulse-to-pulse variations of LIBS signal. If it increases (or decreases), the layer containing an analyte is began (or finished). However, mixing of layers of different materials because of melting and resolidification during a multiple shot depth profiling can lead to worsen the resolution with respect to ablation rate. This means that the changes between two consecutive single shot LIBS spectra cannot reflect the changes in the average depth composition, and the ablation rate will be an inaccurate estimation of depth resolution. Recently, Banerjee and Fedosejevs[98] have introduced a concept of "*depth sensitivity*" to describe an approach to estimation of accuracy for distinguishing the boundary between two-layer system with the use of single-shot LIBS signals of each component. As an example, they have calculated depth sensitivity as "the Cu layer depth where the Si emission falls to 1/e from its pure Si value" for thin Cu-Si interface layer. It was 2.5-4 nm for crater depths of 25-100 nm. This term can be interpreted as a minimal change in depths which can be reliably detected as changes in LIBS signal of the sample constituents. Evidently, the depth sensitivity is preferable as a measure of the ability to perform depth profiling by LIBS

techniques because of simplicity of its measurements compared with ablation rate.

The very first work on application of femtosecond LIBS to measure thickness of multilayered coatings of the Cu–Ag sandwiches was performed by Margetic *et al.*[89] Two types of Cu–Ag samples were prepared by thermal deposition of Cu and Ag layers on a Si wafer: double and triple sandwiches of alternating Cu and Ag layers. The thickness of each copper and silver layer was ~600 nm. For fluence about 1 J/cm² they have detected five boundaries between layers after ~25-30 laser shots. Since the depth profiles of Cu and Ag were constructed by accumulation of 10 pulses, accurate estimation of depth resolution in the term of "depth sensitivity" has to give a larger value of, at least, 200 nm instead of ablation rate of 15-30 nm/pulse. By comparing ns-LIBS with fs-LIBS, Pouli *et al.*[99] have measured the thickness of different types of thin organic films used as protective coatings on historical and archaeological metal objects. They have established that ns pulses were inadequate to profile the polymer coating on Al-Mg substrate because of their weak absorption, while fs pulses yielded well-resolved profiles with depth resolution of 1 μm. More recently, De Bonis *et al.*[100] have also compared 40 ns pulses *vs.* 40 fs pulses to measure depth of a patina in order to clean the corroded bronzes. Since the ablation rate of 40 ns laser ablation was four times larger than for 40 fs laser, the resolution of femtosecond LIBS depth profiling was better, and accuracy for Cu/Sn ratio was better due to the minimal fractionation as well.

Unlike the depth profile with a sharp leap due to interface between two layers, an accuracy problem of LIBS should be overcame to construct "*continuous*" depth profiles. In principal, LIBS is a microdestructive technique[101] indeed because an analyzed material in plasma is removed from a surface. In spite of attempts to analyze the ablated particulates,[102] it is not possible to accurately establish the local composition of the material after it has been removed from sample. Therefore, the one more task is to compare the results of in-depth measurements by LIBS and by other analytical techniques. Accuracy can be proved by in-depth measurements of the same area by non-destructive techniques before ablation. Electron spectroscopy for chemical analysis or Auger electron spectroscopy can be applied for non-destructive profiling of ultrathin layers (0.5-5 nm). For larger sampling depths (up to several μm), there is Rutherford backscattering spectroscopy (RBS) of low mass and high energy ions in the MeV range with depth resolution of about 1-5 nm.[103] RBS depth profiles are infrequently matched to fs-LIBS data because of the cost of technique (required He⁺ source), although it was suitable to determine the thickness of a specific coating or deposition. At the same time in-depth results of LIBS are sometimes compared with other microdestructive techniques such as glow-discharge OES, electron probe microanalysis (EPMA), SIMS, and laser ablation ICP-MS due to their cost and simplicity in comparison with RBS. To assure an accuracy of quantitative analysis, such a comparison demands an assumption on either sample homogeneity or that depth profiles are the same in different

points of sample surface. Recently, Galmed *et al.*[104] have examined the ability of fs-LIBS to make depth profiling for a Ti thin film deposited onto a Si substrate during thermal annealing. They have estimated the thickness of Ti coating measured by after annealing as 213 nm. Because such depth corresponded to the intersection between Si and Ti signals, they have established that LIBS can be considered as the rapid analytical technique to accurately estimate the thickness of coatings.

However, there was the only work on the comparison of a "continuous" profile obtained by fs-LIBS with the in-depth measurements by other techniques. Das *et al.*[105] have also tried to quantitatively locate the interfaces of interdiffusion zone (depth ~20-25 μm) in a thermal barrier coated sample by 150 fs laser pulses with fluence of 18 J/cm$^2$. The average ablation rate was less than 200 nm/pulse. It is interesting to note that each layer was prepared by different techniques: β-(Ni,Pt)Al bond coat was prepared through a combination of electroplating, high temperature diffusion and chemical vapor deposition processes, while ceramic outer layer was deposited on the bod coat by electron beam physical vapor deposition technique. It provided a formation of interdiffusion zone below the bond coat. By comparing fs-LIBS depth profile for Al line with the one obtained by EPMA, they have found that LIBS could indicate the ceramic layer/bond coat interface while the absence of sharp changes in Al intensity across the β layer/interdiffusion zone and interdiffusion zone/substrate interfaces led to the inability of identifying these interface from the spectral intensity profile of Al.

Although it is possible to achieve a very shallow ablation depth per pulse such as ≤2 nm/pulse with the use of ns-LIBS, for example, due to angle-resolved laser ablation[106], the main advantage of femtosecond pulses is still a production of more reproducible craters with the even bottom. By measuring in-depth profiles of Ti ultrathin layers on a steel sheet with the use of doubled 12 ns pulses, Kratochvíl *et al.*[107] have recently shown that the roughness of crater bottom was about 50 nm at depth of 150 nm after single-shot of laser. The technique was capable to measure surface density of Ti on a sheet at the level of several hundreds of pg per mm$^2$ only for single shot because of the etching of Ti layer by first pulse. It means that "depth sensitivity" of fs-LIBS is better, at least, of two orders of values than one provided by ns-LIBS due to the even bottom in a result of low melting.

### 3.2 Lateral resolution

Chemical mapping, i.e. the distribution of a component across a sample surface, requires high spatial resolution, desirably, at near-atomic level or, at least, at nanoscale level. Because of low melting, ultrafast laser pulses being focused onto a sample surface can produce a crater without high rims and other irregularities (*e.g.* droplets) usually observed for nanosecond laser ablation. Therefore, their applications to construct a map are limited by crater size, which is slightly wider than a spot. As it is well known the diffraction-limited beam diameter *d* at the focus of a lens with focal length *f* and aperture *D* is given by a relation:[52]

$$d = \frac{4\lambda f M^2}{\pi n D},$$

where $M^2$ is a propagation constant characterizing the difference from the ideal Gaussian beam, and *n* is a refractive index of the lens. The Gaussian beams give a spot with a minimal diameter (since $M^2 \approx 1$), while the beams with flat-top profiles widely used for in-depth measurements give wider spot because they have $M^2$ value much higher than 10. As a result, the crater diameters are significantly differed and spatial resolution for ablation with flat-top beam is worsened. As an example, Banerjee *et al.*[92] have demonstrated that Gaussian beam provided the production of craters with diameter of ~7-9 μm, while the craters made by flat-top beam had a size of ~90 μm. Since the vast majority of available femtosecond lasers provides a Gaussian distribution across a beam, the several works with such beam profile for mapping can be mentioned: on the sunflower cells,[108] leaves,[109,110] films on silicon[111,112] or aluminium alloys.[113] There are several works on the attempts to real-time micromachining processing on alloys. Tong *et al.*[114] have examined the use of fs-LIBS system as a diagnostics instrument for real-time control of femtosecond micromachining in the process of the fabrication of microheater structures on thermal sprayed materials. Recently, the spectacular demonstration performed by Wessel *et al.*[115] is a searching microcracks or defects in Ti-Al alloys. The spatial resolution of 2 μm allowed the detection of long and narrow cracks and microindentation zones. By comparing SEM and Ti line - LIBS images of an area under investigation, one can see in Fig. 7 that the fs-LIBS allows to detect such a long crack. Due to high repetition rate of fs laser (1 kHz) the operation of mapping does not time-consumable. Another interesting idea related to the chemical mapping by fs-LIBS is to produce precise 3D maps. More recently, Hou *et al.*[116] combined 2D cross-sectional contour maps with layer-by-layer measurements. They obtained the enrichment of two surface layers by Li and Al for the stuffed lithium garnets $Li_7La_3Zr_2O_{12}$. High depth resolution (~700 nm) in the first turn allowed this demonstration, while the lateral resolution was medium (crater size of ~40 μm), although Gaussian beam was used. It may to be noted that an analyte in these cases of fs-LIBS mapping was main or, at least, minor component.

Unlike diffraction-limited beams, non-diffracting Bessel beams have a central core with diameter *d* expressed as:[117]
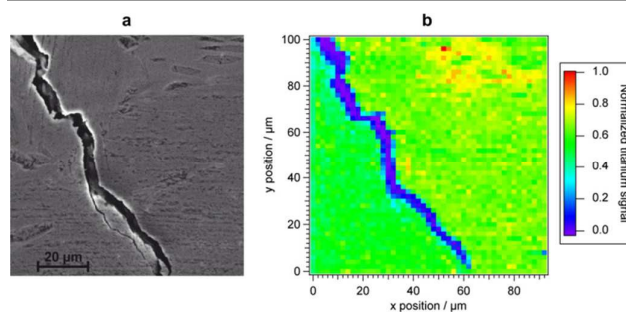


**Fig. 7** (a) SEM micrograph of Ti-Al sample surface before ablation and (b) fs-LIBS map constructed on the intensity of Ti I line. Reproduced from Wessel *et al.*[115] with the permission of Elsevier Science.

$$d = \frac{2.4a}{k(n-1)\tan\alpha},$$

where $a$ is a constant of order unity, $\alpha$ and $n$ are the wedge angle of axicon and its refraction index, respectively. Therefore, the larger wedge angle of axicon is, the narrower crater will be. As an example, Courvoisier *et al.*[96] have recently demonstrated a formation of long channels with diameters of 200 nm and 400 nm that it was smaller than laser wavelength. Moreover, the conical geometry of energy delivery from the rings to the central lobe offers high resistance to filamentation due to nonlinear Kerr effect when compared with Gaussian beams. One more class of laser beams provided high lateral resolution is cylindrical vector beams which are described by a solution to vector Helmholtz equation with cylindrical boundary conditions. The mathematical aspects on cylindrical beams with radial or azimuthal polarization and experimental ways to how generate such vector beam are thoroughly described in comprehensive review of Zhan.[118] The feature of these beams is that polarization direction in vector beams is spatially varies and affects intensity distribution in the focus of high-NA optics. As an example, intensity distributions of a radially (TM) and azimuthally (TE) polarized beam in the focal plane of a NA=0.9 objective are shown in Fig. 8 simulated by Hnatovsky *et al.*[119] SEM images of craters produced by each variant of pulses are given as well. Note that the size of ~0.1λ of the ablated crater produced by the beam possessing a longitudinal z-component of the 30 nJ single TM pulse. So small diameter of the crater provided by either Bessel beams or radially polarized cylindrical vector beams will allow the high spatial resolution for LIBS investigations of sub-micron objects.

To overcome a diffraction limit in far-field optic spectroscopy, near-field microscopy is developed to observe nanometers objects.[120] A main concept of near-field scanning optic microscopy (NSOM) is to place a detector very close to the sample surface at a distance much smaller than the irradiation wavelength. To realize such a configuration, an incident beam passes through a narrow fiber probe (~100 nm), and radiation reflected from a surface collected by the same probe. The first demonstration of NSOM technique capabilities to LIBS measurements was a work of Russo's group.[49] By ablating a silicon wafer with 100 fs 0.18 nJ single laser pulse, they have obtained a crater on silicon wafer with diameter of only 30 nm, but weak LIBS spectrum of silicon was detected with 5.9 nJ pulses produced the crater size of ~1 μm. Next, they could observe the emission lines from sodium and potassium in mica sample by NSOM tool for 40 nJ single pulse; and crater size was ~450 nm.[121,122] The sensitivity of such low energy effect was poor, for example, the average single-shot limit of detection for Na was 2700 ppm. To improve sensitivity, they have exercised in a double-pulse fs-ns scheme for micrometer resolution.[123] By comparing NSOM technology and far-field propagation of cylindrical beam for the LIBS purposes, one can see that the later produces a crater with diameter of ~80 nm, while the former can achieve a ~30 nm craters. However, the energy delivered onto a surface in both cases is strongly differed, indeed, 30 nJ in cylindrical beam *vs.* 0.18 nJ
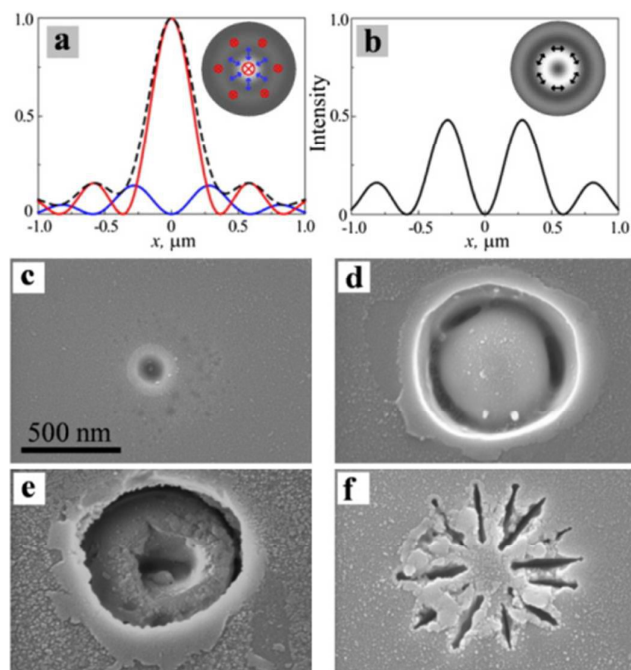


**Fig. 8** (a),(b) Simulated intensity distributions in vacuum of a TM and TE, respectively. SEM images of irradiation of borosilicate Corning 0211 glass samples with (c) the longitudinal component of a 30 nJ single TM pulse; (d) the transverse component of a 120 nJ single TE pulse; (e) multiple 80 nJ TM pulses; and (f) multiple 40 nJ TE pulses. The scale bar is the same for (c)–(f). Reproduced from Hnatovsky *et al.*[119] with permission of American Physical Society.

for NSOM. Since LIBS spectra were detected for 40 nJ in NSOM configuration, the capability of cylindrical beam for higher spatial resolution in LIBS seems to be reasonable.

### 3.3 Signal enhancement in femtosecond LIBS

In the pioneer work[6] on the use of characteristic emission of femtosecond laser plasma for analytical studies the pulse energy did not exceed 400 μJ. Being based on the shown calibration plots it is possible to conclude that the useful signal is roughly comparable with the experimental error in case of the samples containing a few percent of Zn. When comparing the emission properties of laser-induced plasma, generated by pulses of various duration, it was demonstrated that after the period of time of 10 ns the emission intensity is basically determined by the pulse energy.[124] Sabsabi *et al.*[125] used a laser with the energy of 50 mJ. As a consequence, the detection limit of Ag in aluminium alloys was reported to be ~2 ppm at the pulse duration of 80 fs, 2 ps and 270 ps. However, the cost of femtosecond laser systems, giving the energy of dozens of mJ, is much higher. Also, such an advantage of femtosecond evaporation as a small-sized crater with the minimal thermal effects can be implemented when the fluence slightly above ablation threshold. Under these conditions, the spectral lines of the major and some minor constituents are usually observed in the spectra of laser plasma. Although it was shown that emission signal is proportional to pulse energy due to absence of plasma shielding,[126,127] the improvement of sensitivity of fs-LIBS is therefore more urgent compared to

conventional LIBS technique operating with nanosecond lasers. We first consider various options for optimization and improvement of the single pulse scheme.

*Optical configuration.* Location of the focus relative to a surface has a considerable impact on the emission signal, since it influences the crater size, spectral density, and the mechanism of laser breakdown formation. In case of the ns-LIBS, focusing onto the surface of a sample is preferable.[128] In the pioneer work[6] focused on the analysis of brasses it was shown that in case of fs-LIBS the best signal-to-noise ratio was achieved when the focus was located slightly above the surface (so called *prefocus*). Schiffern *et al.*[129] have demonstrated that the highest intensity of Si I line 288.16 nm can be observed at the focucing of the laser beam both under the sample surface (so called *postfocus*) and prefocus depending on fluence. Santos *et al.*[130] have discovered that the maximal intensity of a spectrum of a laser plume from animal tissue is referred to the focus position 1-2 mm below the sample surface.

Scaffidi *et al.*[131] have found out that in case of collinear double-pulse fs-ns LIBS, the highest intensity of a spectrum of pure Fe is observed at the focus position of 2.5 mm both above and below the sample surface. This was in a good agreement with results according to which the maximal signal was detected at the focus of 0.5 mm above/below the surface. Sometimes, the laser beam is focused directly on a surface of samples[132-134] assuming this leads to the maximal fluence and, as a consequence, the highest intensity of spectra.

Finally, Zuhlke *et al.*[135] have performed a fundamental investigation of influence of focusing conditions on fs-LIBS signal of silicon in a vacuum and atmosphere. They found out that in the vacuum conditions (2 Pa) there were two peaks of similar magnitude of Si I 288.16 nm intensity corresponding to pre- and postfocus and local minimum at the focus. At 1 atm the LIBS signal had a single prefocus peak and a continual drop-off in signal through and beyond the focus. This phenomenon was attributed to the continuum generation in air plasma diminishing the energy per pulse and effectively lowering the fluence due to an increase of the total divergence angle in near and post-focus regions. The available data lead to the conclusion that at the optimal fluence for the materials and semiconductors the maximal signal can be achieved at the focusing above the surface. It is also recommended to determine lens-to-sample distance (LSTD) before the analytical measurements. Despite the numerous studies it is still of great importance to continue investigation of fluence and focusing influence on analytical signal as well as on the form and size of craters of dielectric samples.

*Ambient atmosphere.* The nature of gas and its pressure affect significantly on the laser ablation process, laser plasma evolution, and certainly on analytical emission signal. Numerous studies devoted to influence of an ambient atmosphere on ns-ablation have shown that the best sensitivity of LIBS can be achieved at low pressures in the atmosphere of Ar or He depending on the element under investigation.[101] Generally, such an influence on a signal intensity is observed when operating with fs pulses as well,

which is probably related to the fact that in both cases analytical measurements are performed after the end of a laser pulse and plasma for quite a long period of time interacts with atmosphere or expands into vacuum. It was shown that emission signal enhancement and background reduction under low pressures (130-530 Pa) both for lines of main (Al) and minor (Mg) components of aluminum alloys with the use of Ti:Saphire laser (130 fs, 800 nm, 20 μJ).[130] Mateo *et al.*[136] have observed the maximal enhancement of LIBS intensity and SNR for lines of Cu, Zn, Si, Al at 3 kPa measured in copper, brass, silicon and aluminum alloy. The difference in optimal pressure is most likely due to sufficient higher laser energy in the latter case (KrF excimer, 450 fs, 248 nm, 900 μJ). Higher enhancement is observed for argon atmosphere in terms of signal intensity, while the maximum values of SNR are obtained when helium is employed for most of the studied lines. Maximal values of signal intensity or SNR are reached at a half of normal pressure for both helium and argon. Nakimana *et al.*[137] have demonstrated that temperature and electron density of laser-induced plasma determined the signal enhancement of Al and Mg lines under reduced pressure in noble gas atmosphere (50 fs, 800 nm, 3.5 mJ). Hotter and denser plasma was observed in argon than that in air and helium. They also noted that plasma parameters at relative low pressures of argon (1 kPa) are similar to those obtained at relative high pressures of helium (80 kPa). In fact, argon provides the best environment of femtosecond laser-induced breakdown spectroscopy only at relative low pressures while helium constitutes a good environment only at relative high pressures.

A somewhat different situation was described by Harilal *et al.*:[138] though the optimal value of SNR was observed at 2,5-6,5 kPa, the signal intensities were maximal near to half of atmospheric pressure levels. Apparently, this is because the plasma core did not fit into area of the plasma used for observation (1 mm above surface) within selected temporal parameters of registration (delay 100 ns, gate 1 μs). Moreover, the time resolved images of laser plume clearly demonstrated that plasma core has been expanded and moved away fast from the surface under reduced pressure, and maximal intensity of plasma emission was observed significantly higher than 1 mm. To sum up, the ambient atmosphere influences the fs-plasma in the same way as ns-plasma, thus the maximal signal enhancement can be obtain at reduced pressure of noble gases. One should keep in mind that the pulse energy obviously influences the plasma dynamics and, as a consequence, the certain value of optimal pressure value can vary. Most likely, the intensity increase of a certain line depend on electron density and temperature, for instance, the emission intensity of a plasma on a Zn target was maximal at 530-1300 Pa depending on an atomic or ionic line.[139]

*Pulse shaping.* The above mentioned approaches of signal enhancement were not specific for the fs-LIBS, although there were some differences comparing to the ns-LIBS. There are still some phenomena related to the use of femtosecond laser pulses. First of this is regarded to temporal or phase modulation of laser pulse. Gunaratne *et al.*[126] studied influence

of pulse duration, its bandwidth, and phase shaping on LIBS signal during laser ablation of copper and aluminium (35 fs, 800 nm, 750 μJ/pulse). Pulse duration and bandwidth were varied by box shaper and a number of slits, respectively, frequency domain was modified either by sine phase function leading to shift of the mask with respect to the spectrum of the pulse or by applying a variety (512) of binary phase functions. The LIBS signal was relative insensitive to pulse duration, while it was highly dependent on the bandwidth (up to 40% of signal increasing). The effects of sinusoidal and binary modulation showed more modest enhancements with differences between aluminum and copper - in copper non-modified pulses yielded the highest LIBS signal, while aluminum required greater pulse modulation, presumably, due to the aluminum-oxide layer. It also should be noted that pulse shape affected LIBS signal for gentle ablation with pulse energies three to five times above the breakdown threshold, when the intensity was increased to 30 times above the threshold; the effect of modulation was decreased to less than 10%. Guillermin et al.[140] have developed a sophisticated system for pulse shaping including spatial light modulator, which allowed controlled retardation of spectral components, tailoring in turn the temporal shape of the pulse, and closet loop with the feedback to the result of the laser action. They have applied an adaptive optimization loop to lock up temporal shapes to increase the intensity of selected aluminium lines. The optimal pulse shape was attempted to be simplified as two components: a pair of fs-pulses with delays of 5-15 ps and a "long" pulse of 6 ps width. The multiplication factor up to 3.64 was obtained due to the reduction of the neutral species emission by a consequence of femtosecond pulses and augment of the ionic emission by a distribution of energy in the picosecond timescale. The latter also allowed an enhancement of the total luminosity of the plasma. Later the same authors provided additional experimental data and numerical calculations for deep understanding of signal enhancement with shaped pulses.[141] They have demonstrated that optimized pulse shape resulted in the increase of distance from the surface achieved by the front of the plasma, the same temperature (2600 K) *in the vicinity* of the surface, higher excitation state with a smaller area associated with neutrals, a high front temperature (~34 000 K), producing a majority of multiple ionized aluminium atoms, the larger size of Al II area with the density state more than one order of magnitude higher (~$10^{23}$ m$^{-3}$) than for single pulse. The same results were obtained for fs-LIBS study of brass alloy with pulse shape optimization.[142] The regions of neutral and ionized species were formed due to increasing temperature profile together with the corresponding ionization degrees. Neutral Cu and Zn atoms were mainly located in the vicinity of the surface, while closer to the plasma front zone was leaded by ionized ones. Hartig et al.[143] compared the effect of pulse width (45 fs-1.5 ps) and shape resulting from application of both positive and negative chirp on SNR and peak-to-peak signal variations in fs LIBS of copper and uranium. Although the intensities of specific lines depended on both the sign of chirp and the pulse duration, only an increase of 27 % and 18 % in the SNR for

uranium and copper, respectively, was observed compared to the SNR measured at the shortest pulse duration. The SNR and peak intensity were decreased for pulse durations longer than 1 ps regardless of the chirp sign. Thus, on the basis of the relevant papers, we may conclude that pulse shaping can give some enhancement of figures of merit of LIBS measurements, especially if the technique should be adapted to a specific analyte. It also should be noted that the simple pulse width variation does not provide the significant increase of signal or SNR.

*Continuous emission.* We conclude the consideration of the potential merits of fs plasma for analytical measurements with the discussion of a continuous background and its ratio to atomic lines. In earlier works on fs-LIBS, it was noted the relatively low background level in emission spectra. Moreover, it was shown that the combination of non-gated detection of LIBS and high pulse rates, up to 1000 Hz, was effective for increasing the LIBS signal for a given measurement time.[144] Thereafter it was considered as the one of the advantages of fs-LIBS in numerous papers. However, some remarks are needed to get a clear description of the impact of the background on analytical results in fs-LIBS. Firstly, the ablation thresholds are much lower for fs pulses than for ns ones and, as a consequence, the plasma can be generated even with the pulse energy of several μJ. Secondly, the pulse energy is often hundreds of μJ and rarely more than few mJ. This feature together with the absence of beam-plasma interaction is resulted in a relatively low plasma temperature, which is apparently the main reason of low continuum radiation level. Thirdly, the signal enhancement in fs-LIBS is usually studied on individual substances or binary alloys and, therefore, the lines of main components are considered. Taking into account that fs plasma may be denser than ns one, the spectral interference would increase for non-gated registration and lines of minor components can be strongly overlapped with lines of the main component. Actually, Le Drogoff et al.[145] demonstrated theoretically and experimentally that dependence of the continuum emission appears to be similar for different pulse duration (fs to ns) of pulses with high-energy (50 mJ). They concluded that laser-produced plasmas evolve through similar transient states, the only difference being that these states were reached at different delays after the laser shot. Thus the temporal gating parameters are still important for analytical measurements and it is preferable to choose them for each laser pulse duration if possible.

This observation is also in agreement with the study of fs and ns LIBS of brasses of Freeman et al.[146] The intensity of background radiation was high during at least 100 ns after ns pulse, while it became negligible after 25 ns for fs one. Also there were attempts to reduce continuum radiation due to a specific process in fs laser plasma. In particular, Liu et al.[147] reported that continuum emission of the plasma produced in the femtosecond ablation of Si could be polarized. Later the same authors tried to apply this effect to LIBS measurements of aluminium,[148] copper and graphite[149] to cut off continuum emission and enhance signal-to-background ratio (SBR) with the use of polarizer. Unfortunately, mainly scattered laser light

(s- or p-polarized) was removed by polarizer, while only approximately 15% of continuum was polarized due to its reflection by the target surface and polarization of the outgoing radiation in accordance with the Fresnel equations.[150]

*Molecular fragments.* Low temperature of plasma, low thermal effects during ejection of matter, especially near ablation threshold, yield production of molecular fragments of ablated substance. This is evident drawback for most cases of elemental analysis, but it make possible to correlate emission of molecular species to organic content in ablated material.[151] Thus generation of molecular fragments enhance the possibilities of LIBS for organic materials analysis. Primarily, this feature of fs-LIBS was applied for detection explosives on the surface.[152-156] High yield of molecular species is an undoubted improvement of elemental analysis, when molecular form is used. Yee *et al.*[157] have used characteristic molecular spectra of two boron isotopes to reconstruct the boron isotopic ratio by fs-LIBS. More recently, Russo's group[158,159] developing Laser Ablation Molecular Isotopic Spectrometry (LAMIS) suggested to use fs-LIBS for isotopic analysis of five Zr isotopes in the form of their oxides.

*Double pulse.* The use of double pulse (DP) regime is one of the most common and efficient technique for signal enhancement in LIBS.[160,161] The same can be referred to fs LIBS to some extent. The results of studies devoted to the use of DP regime in fs LIBS for signal enhancement are summarized in Table 1. In most cases enhancements factor was calculated as a ratio of line intensity in DP regime to those in SP regime. Although all possible of DP configuration were considered (collinear, orthogonal with pre-spark and reheating one), there are some limitations due to high cost of fs laser and low pulse energy. Firstly, all studies with a pair of fs pulses employed one laser with either temporal shaping of pulse inside laser or optical delay. As a result, a delay varied within the range of 0-1 ns. Secondly, the energy of re-heating fs pulse was relatively low in comparison with ns one. The latter limitation was successfully overcome by the use of additional ns laser, which was reported to be done for the first time by Scaffidi *et al.*[131] Orthogonal ns pulse can deliver enough energy to reheat plasma with the preservation of advantages of fs ablation. Also, such combination provided the highest enhancement of signal intensity up to 360-fold (see Table 1). Collinear scheme can provide much lower signal enhancement, which is presumably to low pulse energy. Unfortunately, the majority of studies with the use of DP regime in fs-LIBS covered only ablation of individual substances and often a monitoring of resonance atomic lines. Thus, the effect of DP on signal enhancement can be mixed with self-absorption and also the possible spectral interference did not evaluated. Only few works, for example Ref.162, examined the influence of DP on figures of merit of analytical procedure. The leading mechanism of signal enhancement can be related to plasma reheating[163] and atomization of nanoparticles,[164] which generation by fs-LIBS was discussed earlier in Part 2.

Besides traditional application of DP for signal enhancement, there is a number of papers[165-168], where the second pulse was used as a probe to study evolution of plasma, including the evaluation of nanoparticle compositions.

### 3.4 Self-absorption

Self-absorption effect is suddenly more strongly for the fs-LIBS technique in comparison with the use of nanosecond pulses. By comparing ablation of copper alloys by 80 fs and 270 ps pulses, Le Drogoff *et al.*[125] have observed the strong deviation of calibration curve for Ag resonance line from linearity in the range of 100-450 ppm. They tried to achieve the best sensitivity with high energy pulses of ~50 mJ/pulse and fluence of ~20 J/cm$^2$ because of the absence of plasma shielding with the use of femtosecond pulses. However, self-reversal of resonance Mg line as well as self-absorption of resonance Ag line were considerably more pronounced as the laser pulse duration was reduced. To explain such a behavior, authors assumed that two reasons acted mutually: higher ablation efficiency of femtosecond laser ablation[169] resulted in higher number density of atoms, while lower plasma temperature[170] made the population density of the ground-state species higher. Elhassan *et al.*[171] have demonstrated similar behavior of Zn/Cu, Sn/Cu, and Pb/Cu ratios for ablation of bronze alloys by 500-fs pulses of 11.2 mJ. In the same time, there were no significant differences in plasma temperature and electron density between nanosecond and femtosecond ablation under their experimental conditions. Fornarini *et al.*[172] have observed that calibration graphs for lead and tin had a tendency to be lower than linear dependences regardless pulse durations. They have used two fs-systems with fluences of 6.5 J/cm$^2$ (8.2 mJ/pulse) and 15 J/cm$^2$ (3.0 mJ/pulse). In this case, authors have attributed their observations to the so-called phenomenon of "*fractionation*" because calibration curves for Zn/Cu ratio were close to linear for nanosecond and femtosecond ablation of bronze alloys. Similarly, Margetic *et al.*[6] have demonstrated the absence of non-linear trend of a calibration curve for Zn/Cu ratio for brass alloys ablation at different pressures and laser fluences. In any way, possible strong self-absorption should be taken into account to choose between fs-LIBS and ns-LIBS as an analytical method.

## 4 Filament-induced breakdown spectrometry (FIBS)

### 4.1 Filament-induced breakdown spectrometry basics

The unique LIBS capability to perform express elemental analysis of remote sample makes this method a very perspective for military and safety application as well as space exploration missions (ChemCam instrument in the Curiosity mission by NASA). But conventional *ns*-LIBS is limited to the distance of a hundred meters due to the difficulty of delivering high laser intensities sufficient to induce ablation and ionization of the remote target. There are two main limiting factors: diffraction on focusing optics and atmosphere optical properties fluctuation. Ideally, lens focal plane should be equal to the distance between laser and sample but even high quality optics suffer from spherical aberrations at several tenth

# Journal Name

## ARTICLE

Table 1. Emission signal enhancement with the use of DP regime [123,127,129,173-200]

| Sample | Analytical Line, nm | Lasers in DP combination | Optical scheme, interpulse delay, other conditions [a] | Enhancement Factor |
|---|---|---|---|---|
| Pure copper | Cu I 515.32 | 100 fs, 800 nm, 6 mJ + 7 ns, 1064-nm, 30 mJ | O (ns spark 1 mm height), 5 μs | 30 |
| | Cu I 324.75 | 80 fs, 800 nm, 1 mJ + 1 mJ | C, 106 ps | 11 |
| | Cu I 324.75 | 120 fs, 800 nm, 50 J/cm$^2$ + 50 J/cm$^2$ | C, 106 ps | 9 |
| | Cu I 510.55, 515.32, 521.82 | 250 fs, 527 nm, 0.6 J/cm$^2$ + 0.6 J/cm$^2$ | C, 2 ns, 200 ps, 10$^{-9}$ bar | 4.5-6.5 |
| | Cu I | 100 fs, 800 mm, 25 μJ + 25 μJ | C, 300 ps, 10$^{-4}$ Pa | 4 |
| | Cu II 490 (unresolved), Cu II 505.18 | 250 fs, 527 nm, 0.6 J/cm$^2$ + 0.6 J/cm$^2$ | C, 2 ns, 200 ps, 10$^{-9}$ bar | 6.5-11 |
| Bronze, brass | Cu I 282.44, 465.11 | 250 fs, 527 nm, 3 mJ + 7 ns, 532 nm, 45 mJ | O (ns spark 0.5 mm height), 8 μs | 70-280 |
| | Cu I 465.11, 510.55, 515.32, 521.82 | 100 fs, 800 nm, 0.5 mJ + 0.5 mJ | C, 27 ps | 3.5-5 |
| | Cu I 521.82 | 100 fs, 800 nm, 10 mJ + 5 ns, 1064-nm, 150 mJ | O (fs spark 0.6 mm height), 3.5 μs | 2.5-4 |
| | Cu I 450.94 | 450 fs, 248 nm, 0.5 mJ + 0.5 mJ | C, 200-400 ps | 9.5 (2[b]) |
| | Zn I 481.05 | 450 fs, 248 nm, 0.5 mJ + 0.5 mJ | C, 200-400 ps | 7.2 (2[b]) |
| | Zn I 481.01, 472.21, 481.05 | 100 fs, 800 nm, 0.5 mJ + 0.5 mJ | C, 27 ps | 3.5-5 |
| | Zn I 472.21 | 250 fs, 527 nm, 3 mJ + 7 ns, 532 nm, 45 mJ | O (ns spark 0.5 mm height), 8 μs | 14 |
| | Sn I 284.00 | 250 fs, 527 nm, 3 mJ + 7 ns, 532 nm, 45 mJ | O (ns spark 0.5 mm height), 8 μs | 30 |
| | Pb I 280.20 | 250 fs, 527 nm, 3 mJ + 7 ns, 532 nm, 45 mJ | O (ns spark 0.5 mm height), 8 μs | 10-15 |
| Pure gold | Au I | 100 fs, 800 mm, 25 μJ + 25 μJ | C, 200 ps, 10$^{-4}$ Pa, | 5.3 |
| Pure aluminum | Al I 394.40, Al I 396.15 | 100 fs, 800 nm, 6 mJ + 7 ns, 1064 nm, 30 mJ | O (ns spark 1 mm height), 5 μs | 80 |
| | Al I 396.15 | 100 fs, 800 nm, 10 mJ + 5 ns, 1064 nm, 150 mJ | O (fs spark 0.6 mm height), 55 μs | 3-3.5 |
| | Al I 394 + 396 (unresolved) | 30 fs, 785 nm, 125 nJ + 125 nJ | C, 800 ps | 6 |
| | Al I 394.4, 396.15 | 150 fs, 800 nm, 0.5 mJ + 0.5 mJ | C, 9 ps, 10$^{-5}$ Pa | 0.5 |
| | Al II 358.7, 466.3, 559.32 | 150 fs, 800 nm, 0.5 mJ + 0.5 mJ | C, 9 ps, 10$^{-5}$ Pa | 1.7-3.5 |
| | Al II 281.62 | 450 fs, 248 nm, 0.5 mJ + 0.5 mJ | C, 400 ps | 5.6 |
| Aluminium alloy | Al I 396.152 | 50 fs, 800 nm, 40 μJ + 40 μJ | C, 150 ps | 4.3 |
| | Al I 396.152 | 50 fs, 800 nm, 40 μJ + 40 μJ | C, 150 ps, Ar jet | 3 |
| | Mg I 518.36 | 50 fs, 800 nm, 40 μJ + 40 μJ | C, 150 ps | 7.5 |
| | Mg I 518.36 | 50 fs, 800 nm, 40 μJ + 40 μJ | C, 150 ps, Ar jet | 2 |
| Pure titanium | integral Ti I (430.6, 445.7, 453.6) | 100 fs, 620 nm, 2 mJ + 2 mJ | C, 0.9 ns, 10$^{-6}$ Torr | 2-7 |
| | Ti I 451.80 | 250 fs, 527 nm, 0.8 mJ + 7 ns, 532 nm, 25 mJ | O (ns spark 1 mm height), 500 μs | 35 |
| | Ti I 453 .3 + 453.5 (unresolved) | 30 fs, 785 nm, 125 nJ + 125 nJ | C, 800 ps | 2.5 |
| | integral Ti II (334.9, 368.5, 375.9, 376.1) | 100 fs, 620 nm, 2 mJ + 2 mJ | C, 0.9 ns, 10$^{-6}$ Torr | 2-7 |
| | Ti II 346.15 | 250 fs, 527 nm, 0.8 mJ + 7 ns, 532 nm, 25 mJ | O (ns spark 1 mm height), 500 μs | 500 |
| | Ti III 251.60 | 250 fs, 527 nm, 0.8 mJ + 7 ns, 532 nm, 25 mJ | O (ns spark 1 mm height), 500 μs | 900 |
| Pure iron | Fe II 274.65 | 450 fs, 248 nm, 0.5 mJ + 0.5 mJ | C, 400 ps | 9.1 |
| Steel | Fe I 438.41, Fe II 419.95 | 350 fs, 257.5 nm, 10 μJ + 1030 nm, 10μJ | C, 40 ps | 3-5 |
| | Cr I 425.48, Cr II 449.71, | 350 fs, 257.5 nm, 10 μJ + 1030 nm, 10μJ | C, 40 ps | 3-5 |
| CMSX-4 superalloy | Ni I 352.45 | 150 fs, 775 nm, 160 μJ + 640 μJ | O (2$^{nd}$ fs spark 30 μm height), 10.36 ns | ~500[c] (9[b]) |
| | Cr I 425.44 | 150 fs, 775 nm, 160 μJ + 640 μJ | O (2$^{nd}$ fs spark 30 μm height), 10.36 ns | ~500[c] (9[b]) |
| | Al I 394.40 | 150 fs, 775 nm, 160 μJ + 640 μJ | O (2$^{nd}$ fs spark 30 μm height), 10.36 ns | ~500[c] (9[b]) |
| Pure nickel | Ni I 447.047, 464.865, 478.653, 547.691 | 33 fs, 810 nm, 0.2 mJ + 0.2 mJ | C, 50 ps | 5-13 |
| Bilayer Ag/Al plate | Al I 394.40, 396.15 | 60 fs, 800 nm, 0.3-30 μJ + 0.3-30 μJ | C, 104 ps | 7-3.5 |
| | Ag I 405.85, 421.62, 431.32, 520.91, 546.54 | 60 fs, 800 nm, 0.3-30 μJ + 0.3-30 μJ | C, 104 ps | 13-3 |
| Pure silicon | Si I 288.16 | 450 fs, 248 nm, 0.5 mJ + 0.5 mJ | C, 400 ps | 4.3 |
| | Si I 288.16 | 800 μJ pulses with 50 fs, 800 nm, 125 μJ + 125 μJ | C, 0-80 ps | 1.1-2 |
| | Si I288.16 | 100 fs, 800 nm, 28 μJ + 28 μJ | C, 60 ps | 2 |
| | Si I 212.41, 221.67, 243.52, 251.61, 288.16 | 100 fs, 800 nm, 1 mJ + 1 mJ | C, 70 ps | 1.2[d] |
| | Si II 505.6 | 80 fs, 800 nm, 1 mJ + 1 mJ | C, 106 ps | 6 |
| | Si II 505.6 | 100 fs, 800 nm, 28 μJ + 28 μJ | C, 60 ps | 2 |

| Single-crystalline silicon | Si I 252 (unresoved), 288.16 | 500 fs, 343 nm, 400 nJ + 6 ns, 355 nm, 1.5-3 mJ | O (ns spark 45 µm height), 500 ns | 360 |
|---|---|---|---|---|
| Pure boron | B II 412, 477, 497, 700 | 150 fs, 800 nm, 0.5 mJ + 0.5 mJ | C, 15 ps, $10^{-5}$ Pa | 1-1.4 |
| $BaSO_4$ | Ba II 455.40 | 450 fs, 248 nm, 0.5 mJ + 0.5 mJ | C, 400 ps | 8.1 |
| $CaF_2$ | Ca II 317.93 | 80 fs, 800 nm, 1 mJ + 1 mJ | C, 106 ps | 2 |
| $Gd_2O_3$ | Gd I 419.08, Gd II 409.86 | 100 fs, 800 nm, 2 mJ + 532 nm, 10 ns, 30 mJ. | O (ns spark 0.9 mm height), 2-4 µs | 10-25 |
| Polymethyl methacrylate - PMMA | Ca II 393.4, 396.8 | 45 fs, 800, 300 µJ + 300 µJ | C, 80 ps | 6.5 |
| | Ca I 422.6, Na I 589.0, 589.6 | 45 fs, 800, 300 µJ + 300 µJ | C, 80 ps | 4 |
| | CN 388.3, $C_2$ 516.5 | 45 fs, 800, 300 µJ + 300 µJ | C, 80 ps | 2 |
| | CH 431.4 | 45 fs, 800, 300 µJ + 300 µJ | C, 80 ps | 1.5 |
| Air | Intensity at 400, 450, 500 | 120 fs, 800nm, 86 µJ + 26 µJ | C, 40 ps | 5 |
| | N II 500.5, | 33 fs, 810 nm, 0.8 mJ + 1.0 mJ | O, 0 fs | 32 |
| | H I 656.2, | 33 fs, 810 nm, 0.8 mJ + 1.0 mJ | O, 0 fs | 8 |
| | N I 746.8, | 33 fs, 810 nm, 0.8 mJ + 1.0 mJ | O, 0 fs | 7.5 |
| | O I 777.2 | 33 fs, 810 nm, 0.8 mJ + 1.0 mJ | O, 0 fs | 6 |

[a] O – orthogonal scheme, C – collinear scheme. [b] This value was obtained in terms of decrease of a signal detection threshold. [c] This value was obtained near ablation threshold. [d] in terms of electron density and excitation temperature.

meters distance. To overcome this, the large size and heavy optics system should be constructed that limits mobility of remote LIBS system. Second problem that can't be principally solved even with ideal optical system is a fluctuation of atmosphere optical properties for tenth meters optical path. Air refraction index fluctuation (turbulence vortexes) generally combined with aerosol particle movement that together completely distort laser beam at a distance of several tenth meters.[201] Increasing the efficiency and measurement range and improving signal-to-noise ratio are important issues for LIBS applications.

To the our best knowledge, conventional remote sensing of solid target by fs laser pulses was only studied by Rohwetter *et al.*[202] They used positive chirping to reach enough fluence without filamentation. Such a variant of remote LIBS seems to be not perspective because no benefits will be achieved compared to nanosecond remote LIBS with sufficient increase in complexity and cost of the fs system. A new era of laser remote elemental analysis have been started when filaments were used to produce plasma on solid sample surface. The capability of filamentation to overcome diffraction limit and deliver high laser intensities at long distances without focusing have been demonstrated in the early 2000s.[39203204] But first application[205] of filaments to induce laser plasma remotely was made by Teramobile team in 2004 for sample located at a distance of 90 m. Teramobile system consists of a terra-watt laser and a detection system installed in a 20-foot standard freight container allowing field measurement campaigns. A detailed description of the system and main results of the project can be found in numerous papers[206,206,207,208,209,210,211] as well as at Teramobile's official site.[212]

Thereafter, such a variant of LIBS more frequently is named filament induced breakdown spectrometry (FIBS), and we also will use this term in this review. In the above mentioned pioneer work the femtosecond non-focused laser beam (800 nm, 80 fs, 250 mJ) initiated multiple filaments (up to 30) at 7 m before the pure metal samples (*Cu* and *Al*), which was located 90 m from the system.[205] Filament induced plasma emission

was collected by 20 cm telescope and guided to spectrograph equipped with gated detector. The spectra revealed absence of broad-band emission within the first 100 ns that indicated low temperature and electron density of the plasma. Atomic lines of *Cu I* and *Fe I* were clearly observed with better contrast compared to nanosecond LIBS system. In the next Teramobile paper on FIBS[213] a length and initiation point of filament before target was optimized by varying beam diameter and chirp. Line emission from a metallic target was registered at distances up to 180 m from the laser. Moreover, authors assumed that this distance can be extended up to 1 km and is restricted by collecting optics and detector efficiency only. This is the principal advantage of FIBS over remote ns LIBS systems with laser beam focusing, which is of great interest for remote sensing of dangerous or unreachable sites like explosives or chemical pollutants.

### 4.2 Filament induced ablation

Filament induced ablation can be defined as ablation of solid/liquid surface by femtosecond pulse with power density above filamentation threshold in surrounding media. In other words ablation is induced by both filaments and femtosecond laser pulse. It should be noted, that filaments contain only a small fraction of energy compared to laser pulse (less than 1%)[21,36,205] but plasma channels (filaments) change laser matter interaction. The majority of papers on FIBS were focused on feasibility proof of remote analysis for different types of samples, i.e. detection of atomic/molecular spectra from large distance for major sample components. The physics of filament induced ablation and resulting plasma have been studied superficially in a few papers.

**Crater** studies were carried out for 5 cm diameter femtosecond laser beam that ablated remote copper target.[213] A multiple craters (up to 30) with 100-200 µm diameters were formed by individual filaments. Authors studied influence of optical path length on crater properties. They compared craters produced on metallic plates located at 25 and 90 m from laser by a beam producing multiple filaments (each ~100

ARTICLE

μm in diameter). The diameter of first crater was about 5 mm (compare with 50 mm laser beam at laser output) while second crater diameter was significantly larger (about 30 mm). Authors explained it with random walk of filament around its mean position due to fluctuations in air and stochastic nature of multifilamentation. For smaller distances (up to 50 m) and air laboratory conditions crater diameter didn't change as was shown for filament induced (800 nm, 180 fs, 25 mJ) ablation of *GaAs*.[214] A direct comparison of femtosecond and filament induced ablation has been carried out by Valenzuela *et al.*[215] Under the same experiment conditions Ti:sapphire laser pulses (800 nm, 100 fs, 25 mJ) were sharply focused (no filamentation), slightly focused (assisted filamentation) and self-focused (filamentation) on steel and titanium targets. Crater study revealed substantial decrease of evaporated mass for filament induced ablation compared to femtosecond (sharply focused) ablation.

**Plasma emission duration** didn't exceed several hundred nanosecond compared to a few microseconds time scale for non-filament ablation by femtosecond or nanosecond pulses. For example, filament induced plasma on copper target could be detectable at a period of first 130 ns (conditions: 800 nm, 80 fs, 250 mJ/pulse, 10 Hz), which didn't depend significantly on distance between laser and target. [213]For organic films samples a twelve times longer plasma emission duration (1 μs) laser wavelength was observed.[216]

**Broadband emission** for femtosecond induced plasma is significantly lower compared to pico/nano second cases.[202] But FIBS provided smallest continuum background emission compared to fs/pico/nano second pulses.[205,217] First, fs-LIBS provide colder plasma with faster decay compared to ns-LIBS.[146] Second, electron density in filaments is two-three orders lower compared to fs-LIBS thus reducing broadband emission from plasma. The continuum emission for filament induced plasma can be originated from supercontinuum generation during filament propagation in air. Nevertheless, supercontinuum emission spreads within a narrow cone and its intensity is linearly proportional to the propagation distance. Consequently, this process can be effectively controlled by chirping technique (see further in the text). Additionally, the background emission level can be substantially decreased when strong and short filaments are formed to induce plasma thus even a non-gated detectors can be used.[217]

Filament induced plasma **temperature** and **electron density** was measured by Xu *et al.*[218] Plasma emission was detected within 200 ns that was comparable to femtosecond induced plasma. The electron density was measured by Stark broadening of *Pb I* lines to drop within a 200 ns from $8\times10^{17}$ to $1\times10^{17}$ cm$^{-3}$. Plasma temperature was detected by Boltzmann plot method decreased from 7000 to 4500 K during the first 100 ns. Judge *et al.*[219] studied plasma temperature induced by a filament on composite graphite samples at a distance of 6 m. A significant difference in plasma temperature calculated by atomic lines (*Al I*, *K I*) and molecular bands of $C_2$ (Swan system) was discovered: 9000 *vs* 5500 K, respectively. Authors explained this fact by non-equilibrium plasmas formed on

different micro domains in the samples superimposed by multiple filaments.

Ambient **air properties** (air turbulences, aerosol conditions, etc.) influenced filament properties and consequently filament induced plasma. Total area of sampling by multiple filaments strongly depends on air turbulences.[213,214] The influence of temperature, pressure, humidity and precipitation (snow) on FIBS signals have been carried out by Xu *et al.*[220] A compact laser system was tested to perform FIBS study under polar conditions. Femtosecond laser pulses (800 nm, 45 fs, 225 mJ) induced filaments in air at temperature below -10 $^0$C under clear sky and snowing conditions. Strong turbulence of air was observed due to 40 degree temperature gradient between measuring system and target. Also a dense snow fall and a weak fog lowered air visibility down to 3.2 km and, therefore, significantly suppressed measured signals. Despite heavy conditions resonance Al I lines were detected with high signal-to-noise ratio at a distance of 60 m. The maximum distance was estimated as 730 m for clear-sky conditions.

### 4.3 Optimizing filament induced breakdown spectrometry

*Laser wavelength.* Although, near infrared (IR) Ti:sapphire lasers are common for FIBS due to their availability, there are a few studies with ultraviolet (UV) ones. The results of impact on the plasma properties are contradictory. UV filament ablation resulted in more effective atomization and molecule collapse in case of complex inorganic or organic material,[221] while sufficient increase of molecular fragments (*CN*, *NH$_2$*) formation in comparison with IR radiation was observed for dinitrotoluene and ammonium perchlorate, respectively.[222] It is obvious that systematic study of mechanisms of wavelength influence on the filament induced ablation would be extremely desirable.

*Pulse chirping.* Tuning of pulse chirping allows precise control of the filament initiation.[21] The optimization of chirping was performed by Rohwetter *et al.*[213] A detailed experimental studies (800 nm, 80 fs, 250 mJ/pulse, 10 Hz) revealed that filament induced plasma atomic emission increases significantly if filament initiated several meters before the target. The optimal chirp duration was explained by the dynamic nature of multiple filamentation.

Laser beam energy is not effectively used for excitation of filament induced plasma due to defocusing and lowering peak intensity of laser beam at filament clamps, resulting tiny conversion of pulse energy into plasma. Zeng et al.[223] suggested a spatio-temporal chirping to increase peak intensity in filament core. Two cylindrical lenses (concave and convex) inside a laser confined beam to elliptical profile. The filament length was significantly shorter than for initial laser beam. This was explained by spatial separation of different components at focus and chirp free pulse in focal spot. Nitrogen molecule ionization increased in a one order of magnitude in filament core. The suggested technique can be of great interest to improve spatial resolution for LIDAR applications while the capability of filament initiation at any position for long distances is keeping. The same authors observed[224] a significant (3-5 times) intensity increase of

# Journal Name

## ARTICLE

**Table 2**. Remote sensing applications by filament induced fluorescence and plasma spectroscopies. For better view the data was sorted for laser to sample distance ascending.

| Analyte | Matrix | Distance (estimated)*, m | Laser parameters | Conditions | Reference |
|---|---|---|---|---|---|
| Cu I  Fe I | copper  steel | 180 (up to 1000) | 800 nm, 80 fs, 250 mJ | open air; field conditions | 205, 213 |
| Al I | aluminum | 60 (730) | 800 nm, 45 fs, 225 mJ | open air, – 20 $^0$C, snowing | 220 |
| Al I, Mg II | aluminum | 50 (1900) | 800 nm, 90 fs, 108 mJ | lab air | 217 |
| Ca I, PH$_2$, NH$_2$, CN | white egg, yeast | 50 (1500) | 800 nm, 45 fs, 7 mJ | lab air | 225 |
| K I, Al I, C$_2$ | composite graphite | 6 | 800 nm, 60 fs, 3 mJ | lab air | 219 |
| Mg I | white marble, red clay | 6 (not estimated) | 248 nm, 450 fs, 20 mJ | air | 221 |
| Pb I | lead | 5 (325) | 800 nm, 45 fs, 12 mJ | lab air | 218 |
| Cr I | leaves, soil | 0.95-1.03 | 800 nm, 50 fs, 4 mJ | lab air | |
| Si I, Mg I, Ca I, Al I, C$_2$, CN | corn, barley wheat | 4 (not estimated) | 800 nm, 45 fs, 12 mJ | air; laboratory conditions | 226 |
| CN  NH$_2$ | dinitrotoluene, ammonium perchlorate | 1.5 (not estimated) | 266 and 800 nm, 100 fs, 15 mJ | lab air | 222 |

*Experiment distance between laser system and sample is presented in first line while estimated maximum distance is shown in brackets.

atomic lines of Al and Fe with the use of spatial-temporal chirped pulse (800 nm, 50 fs, 8 mJ) for FIBS of aluminum and steel sample. Consequently, the spatio-temporal chirping technique allows sending filament at longer distances and more effective conversion of laser energy.

**Focusing optics.** Alternative way for is to use focusing optics to control filament initiation at short range distance (less than 500 m). Formation of short and intense filaments near the target resulted in the low-level continuum emission of plasma allowing the use of non-gated detectors.[217]

### 4.4 Applications

The most applications of FIBS are associated with the unique capability of filamentation to conserve laser beam divergence without any optical systems at the distances up to 20 km.[28] Moreover, it was demonstrated that remote analysis of distant object can be performed by FIBS even under snow conditions.[220]

**Filament induced breakdown spectrometry applications.** Teramobile team initiated the appearance of FIBS by demonstration of plasma formation with filament on remote target.[205] In subsequent publications they tested a variety of pure metals (Al, Ti, *etc.*) as a target, while other research groups focused on various complex samples like biological or cultural heritage objects. The main experimental parameters and results on remote sensing by filaments are summarized in the Table 2.

Tzortzakis *et al.*[221] made the first step towards FIBS analysis of **cultural heritage** studying elemental composition of the

typical materials of sculptures and large monuments (white marble, red clay, limestone, etc.) at the distance 4.5 m. Authors were able to distinguish these materials by small differences in spectral features (for example, Mg I lines for red clay).

The feasibility of FIBS classification of **biological objects** was described in Ref.225. The egg white and yeast were sampled by filaments at a distance of 6 m. The spectra had low level of broadband emission (continuum) and contained atomic lines (Ca, Na) and molecular bands (NH$_2$, PH$_2$, CN) of major components. The more complex goal of agricultural samples differentiation (wheat, barley and corn) by FIBS was challenged in Ref.226. Samples were pressed in pellets and then were sampled by FIBS at a distance of 4 m. The spectra were quit similar (C$_2$ and CN molecular bands and Si, C, Mg, Al, Na, Ca, Mn, Fe, Sr and K lines) due to almost the same elemental composition. Still authors were able to distinguish three types of samples by intensity ratios in the plasma spectra. Recently it was demonstrated that FIBS can be used for monitoring of toxic metals like Cr in leaves[227] and soils[228], but only short distance (~1 m) was tested.

Detection of **explosive material** (dinitrotoluene, ammonium perchlorate) on metal plates by UV FIBS was demonstrated in Ref.222. Molecular bands of CN and NH$_2$ were detected at a distance of 50 m. However authors have not provided any attempts to identify explosive/non-explosive materials by FIBS. Another team has tried to identify organic film as a test samples for explosives material detection.[216] Two polymer namely poly methyl methacrylate (PMMA) and

**ARTICLE**

futurex were ablated by filament in air. Surprisingly authors have detected strong CN molecule bands without any nitrogen molecular emission in PMMA plasma spectra. These results indicates that despite unique capability to induce plasma at long distances by filaments a lot of work should be done for meaningful explosive discrimination by FIBS.

*Isotopic analysis* of zirconium by FIBS was recently performed at a distance up to 7 m by Russo's group.[159] Besides semi-quantitative isotopic analysis without the use of calibration standards, they have investigated the plasma properties generated at different filament propagation distances.

*Filament induced fluorescence spectrometry applications.* The very close to FIBS and perspective application of filament is the use of plasma initiation in atmosphere itself to study fluorescence of gas species. Multigas pollutants at sub-ppm level were quantitatively detected by this technique (800 nm, 45 fs, 6 mJ).[229] Mixtures were analyzed by using a genetic algorithm, showing a good concentration agreement within an error of 25% Laboratory *vs* field measurements of methane in air was directly compared at a distance of 10 to 30 m.[230] Authors detected at least 1% $CH_4$ additive to air at 20 m distance with filaments produced by Ti:sapphire laser (800 nm, 45 fs, 190 mJ, 10 Hz) in laboratory, while field measurements in open air have shown the worse results of $CH_4$ analysis (reproducibility, sensitivity) due to a strong influence of turbulence vortexes on filament formation. Filament induced fluorescence spectrometry was proved to be an effective tool for detecting different objects: gases,[231] water clouds,[232] and aerosols.[233] A series of review paper can be recommended for further reading on remote sensing of gases by filaments.[21,234,235]

## 5 Conclusion

In conclusion, femtosecond laser pulses were believed to provide a brighter future for numerous LIBS applications: absence of fractionation; improved spatial resolution; lower ablation threshold; *etc.* It can be useful for application, where minimal invasion is required, such as analysis of artefacts[171,236-237238] and biological samples,[239] or even bacteria classification[240,241]. Besides this, fs-LIBS technique can be successfully used as an assistant monitoring tool in such application as micromachining or surgery,[242,243] where fs lasers used. But until now, femtosecond laser systems with single pulse energy in a few mJ range are still too expensive and too complex for conventional LIBS measurements. Since femtosecond laser provides low ablation threshold, plasma near threshold has low level of background emission unlike nanosecond ablation, one could expect the improvement of LIBS sensitivity in term of better limits of detection (LOD). Typical repetition rate of femtosecond lasers is in kHz range thus long exposure time of non-gated detector can be applied to sum thousands spectra in CCD matrix during several seconds, which significantly increases signal-to-noise ratio thus

**Table 3** Comparison of the best LODs (in ppm) known for femtosecond and nanosecond single-pulse LIBS. Total number of laser shots delivered to a sample and used to accumulate spectra is given in the brackets.

| Element | Femtosecond LIBS | | | Nanosecond LIBS | | |
|---|---|---|---|---|---|---|
| **Alloys** | | | | | | |
| Ag | 1.4 | | | 0.2 | | |
| Cu | 3.2 | 50 mJ (400) | Ref.125 | 1 | 60 mJ (100) | Ref.244 |
| Si | 30 | | | 8 | | |
| Ni | 10 | | | 7 | 60 mJ (1000) | Ref.245 |
| Fe | 22 | | | 3.7 | 60 mJ (100) | Ref.244 |
| Mg | 2.1 | 50 mJ (100) | Ref.170 | 0.13 | 60 mJ (1000) | Ref.245 |
| Mn | 6.7 | | | 2 | 60 mJ (50) | Ref.246 |
| **Water** | | | | | | |
| Al | 0.19 | | | 0.7 | ≤100 mJ | Ref.248 |
| Ca | 0.01 | | | 0.003 | 16 mJ (12) | Ref.249 |
| Mg | 1 | 1.1 mJ (4000) | Ref.247 | 0.1 | 150 mJ () | Ref. 250 |
| Na | 0.0009 | | | 0.0004 | 16 mJ (12) | Ref.249 |
| Zn | 2.5 | | | 0.05 | 14 mJ (30) | Ref.251 |
| Ba | 0.08 | | | 0.007 | 16 mJ (12) | Ref.249 |
| Cu | 0.78 | 1 mJ (4000) | Ref.252 | 0.39 | 90 mJ (500) | Ref.253 |
| Fe | 2.6 | 7 mJ (10000) | Ref.254 | 37 | 40 mJ (100) | Ref.255 |
| **Tissue** | | | | | | |
| Al | 29 | 840 µJ (500) | Ref.256 | 0.82 | 80 mJ (1200) | Ref.257 |
| **Thin films or coatings** | | | | | | |
| Mg | 3010 | 221 µJ (1) | Ref.258 | 0.24 | 90 mJ (200) | Ref.259 |
| **Leaves** | | | | | | |
| Ca | 0.007 | | | 0.007 | | |
| Cu | 7 | | | 1 | | |
| Fe | 12 | | | 3 | | |
| Mg | 0.02 | 1.5 mJ (15) | Ref.260 | 0.01 | 70 mJ (15) | Ref.260 |
| Mn | 2 | | | 1 | | |
| P | 0.4 | | | 0.1 | | |
| Zn | 80 | | | 4 | | |

improving sensitivity of fs-LIBS. However, lower plasma temperature and shorter plasma life of fs-LIBS should limit the total intensity. In Table 3 we collected the best LODs available in the literature to weigh the pros and cons of detection capabilities fs- and ns-LIBS. To avoid matrix effects under the consideration we gathered values of LOD for matrixes matched as close as possible. For example, LODs given for "*Thin films or coatings*" were retrieved for films of oil or other coatings on the substrate. Moreover, such a division allows the elimination of spectral interferences of main components. Indeed, the comparison of LODs for Mn between Cu alloys for fs-LIBS and Fe-alloys for ns-LIBS seems to be unreasonable. We have also tried to gather the values obtained for the same analytical line of element. However, several elements (such as Fe) are presented by different lines. Since there are many offers to enhance LIBS sensitivity, in Table 3 data of single-pulse LIBS are given only to avoid wrong comparison between techniques. It means that no values for double-pulse technique, laser-induced fluorescence, resonant ablation or sorption on a specific matter, *etc.* are listed. Because no values of laser fluence are given by some authors, we compared laser energy per pulse only. Fs-LIBS at approximately the same pulse energy has, in general, the higher values of LODs than ns-LIBS in spite of the higher ablation efficiency, i.e. sensitivity of fs-

LIBS is, at least, the same for ns-LIBS. Therefore, such an expensive tool as fs-LIBS can not be considered as the best practical way to improve sensitivity.

Improved resolution in 2D and 3D mapping applications was demonstrated by fs-LIBS. Conventional ns-LIBS system under the best conditions can provide spatial resolution of ~50 μm.[261] Other problems associated with "long" laser pulse are the thermal ablation effects and higher ablation threshold responsible for "*matrix effects*". As a result, spatial resolution for ns-LIBS is limited by materials, their surface morphology and compositions,[262] *etc.* Craters with sizes less than diffraction limited laser beam diameters can be produced since the absence of heat-affected zone for femtosecond laser ablation. NSOM technology combined with femtosecond laser can achieve crater diameter down to 450 nm[121] for which fs-LIBS spectrum is still visible. Wonderful achievements in operating with ultrafast laser beams, especially cylindrical vector beams,[119] give expectations of a new breakthrough for fs-LIBS with spatial resolution below 80 nm. Another unique capability of fs-LIBS is high-resolution depth profiling of layers or coatings. For example, a depth sensitivity about 3 nm[98] have been recently reported for thickness measurements of buried layers. However, either high depth sensitivity or high spatial resolution can be achieved in fs-LIBS. So, Gaussian beam provides small and deep craters, while flat-top beam produces wider and shallower ablation craters. It should be noted that the higher spatial resolution is, the lower sensitivity will be because the smaller and smaller mass (and number of atoms) is ablated with concentration of beam energy in a space.

In spite of poor detectability of single pulse fs-LIBS, the spatial resolution allows microanalytical measurements so gentle to provide a low sample damage. For example, fs-LIBS was recently examined for the detection of cancer antigen 125 in blood plasma.[263] The combination of the efficient energy coupling and lower ablation threshold for femtosecond laser sampling is very perspective for analysis of biological materials, such as bacteria, cells, leaves, *etc.* and cultural heritage objects, such as ceramics, bronze statues, glasses and coatings, *etc.* where small damage is of primary interest. Fs-LIBS can also be an auxiliary tool to monitor material processing by femtosecond lasers for cleaning of corroded alloys, preparing sub-micron grooves on a layered surface, *etc.* In this case, LIBS provides a spectral information about stopping or continuing material processing.

The low emissivity of plasma due to relatively low fs laser pulse energy can be overcome by the use of additional ns laser in orthogonal configuration, which can deliver enough energy to reheat plasma with the preservation of advantages of fs ablation.

A new era of laser remote sensing have been started by filament induced breakdown spectrometry (FIBS) utilizing the unique capability of powerful femtosecond laser pulses to initiate filamentation in air. Filamentation makes possible to overcome laser beam diffraction and to conserve laser beam diameter at long distances (up to 20 km) without any focusing optics. This allows delivering laser pulses with high power density needed to induce ablation of remote samples. Conventional focusing systems for remote LIBS utilize focusing optics to achieve power density needed for analytical meaningful plasma. Ideally, lens focal length should be proportional to the distance between laser and sample that resulted in large dimension and mass of optical system. Nevertheless, even ideal focusing optics can not deliver sufficiently powerful laser beam at a distance beyond several tenth meters due to atmosphere properties fluctuation (refraction index fluctuation and interaction with aerosol particles). Filamentation allows delivering laser beam with enough power density to induce plasma breakdown even under heavy meteorological conditions (snowing). Currently, maximum distance for FIBS measurements is determined by collecting optics efficiency and detector system sensitivity. It was demonstrated that the state-of-art FIBS systems can perform measurements at ~200 m distance while maximum estimated distance can reach up to 2 km with appearance of more sensitive gated detectors.

Feasibility of elemental remote sensing by filaments was demonstrated for metallic, inorganic and organic samples. FIBS measurements published in the literature were motivated by remote sensing of dangerous materials (explosives, drugs, *etc.*), cultural heritage objects, and isotopic analysis. So far, FIBS studies were mainly focused on feasibility demonstration rather than on quantitative analysis. The analytical figures of merits for FIBS were roughly estimated at tenth ppm level in one paper presented in the literature.[217] The estimated limits of detection was at tenth to hundreds ppm level for additives in aluminum samples located at distance of 50 m. High cost and complexity of powerful femtosecond laser systems are the main limiting factors for deployment filament induced breakdown spectrometry in everyday practice.

## Acknowledgements

## References

1   C.V. Shank and E.P. Ippen, Sub-picosecond kilowatt pulses from a mode locked cw dye laser, *Appl. Phys. Lett.*, 1974, **24**, 373.

2   P.F. Moulton, Ti-doped Sapphire Tunable Solid State Laser, *Opt. News*, 1982, **8**, 9.

3   D. Strickland and G. Mourou, Compression of amplified chirped optical pulses, *Opt. Commun.*, 1985, **56**, 219.

4   J.A. Cobble, G.A. Kyrala, A.A. Hauer, A.J. Taylor, C.C. Gomez, N.D. Delamater and G.T. Schappert, Kilovolt x-ray spectroscopy of a subpicosecond-laser-excited source, *Phys. Rev. A*, 1989, **39**, 454.

5   B.-M. Kim, M.D. Feit, A.M. Rubenchik, B.M. Mammini and L.B. Da Silva, Optical feedback signal for ultrashort laser pulse ablation of tissue, *Appl. Surf. Sci.*, 1998, **127–129**, 857.

6   V. Margetic, A. Pakulev, A. Stockhaus, M. Bolshov, K. Niemax and R. Hergenroder, A comparison of nanosecond and femtosecond laser-induced plasma spectroscopy of brass samples, *Spectrochim. Acta Part B*, 2000, **55**, 1771.

7   E.L. Gurevich and R. Hergenröder, Femtosecond laser-induced breakdown spectroscopy: Physics, applications, and perspectives, *Appl. Spectrosc.*, 2007, **61**, 233A.

8   J. Herrmann, Theory of Kerr-lens mode-locking - role of self-focusing and radially varying gain, *J. Opt. Soc. Am. B*, 1994, **11**, 498.

9   *Femtosecond Laser Pulses. Principles and Experiments*, ed. C. Rulliere, Springer-Verlag, 2005.

10  K. Yamane, Z. Zhang, K. Oka, R. Morita, M. Yamashita and A. Suguro, Optical pulse compression to 3.4 fs in the monocycle region by feedback phase compensation, *Opt. Lett.*, 2003, **28**, 2258.

11  G. Steinmeyer and G. Stibenz, Generation of sub-4-fs pulses via compression of a white-light continuum using only chirped mirrors, *Appl. Phys. B*, 2006, **82**, 175.

12  O.A. Konoplev, Temporal high-contrast structure of ultrashort pulses: A plea for standardization of nomenclature and conventions, *Proc. SPIE*, 2000, **3934**, 102.

13  S. Fourmaux, S. Payeur, S. Buffechoux, P. Lassonde, C. St-Pierre, F. Martin and J.C. Kieffer, Pedestal cleaning for high laser pulse contrast ratio with a 100 TW class laser system, *Opt. Express*, 2011, **19**, 8486.

14  V.V. Semak, J.G. Thomas and B.R. Campbell, Drilling of steel and HgCdTe with the femtosecond pulses produced by a commercial laser system, *J. Phys. D*, 2004, **37**, 2925.

15  R.Y. Chiao, E. Garmire and C.H. Townes, Self-trapping of optical beams, *Phys. Rev. Lett.*, 1964, **13**, 479.

16  N.F. Pilipetskii and A.R. Rustamov, Observation of self-focusing of light in liquids, *JETP Lett. USSR*, 1965, **2**, 55.

17  A. Braun, G. Korn, X. Liu, D. Du, J. Squier and G. Mourou, Self-channeling of high-peak-power femtosecond laser pulses in air, *Opt. Lett.*, 1995, **20**, 73.

18  P. Béjot and J. Kasparian, Conical emission from laser filaments and higher-order Kerr effect in air, *Opt. Lett.*, 2011 **36**, 4812.

19  V.P. Kandidov, O.G. Kosareva and A.A Koltun, Nonlinear-optical transformation of a high-power femtosecond laser pulse in air, *Quantum Electron.*, 2003, **33**, 69.

20  Y.E. Geints and A.A. Zemlyanov, Self-focusing of a focused femtosecond laser pulse in air, *Appl. Phys. B*, 2010, **101**, 735.

21  S.L. Chin, T.J. Wang, C. Marceau, J. Wu, J.S. Liu, O. Kosareva, N. Panov, Y.P. Chen, J.F. Daigle, S. Yuan, A. Azarm, W.W. Liu, T. Seideman, H.P. Zeng, M. Richardson, R. Li and Z.Z. Xu, Advances in intense femtosecond laser filamentation in air, *Laser Phys.*, 2012, **22**, 1.

22  A. Couairon and A. Mysyrowicz, Femtosecond filamentation in transparent media, *Phys. Rep.*, 2007, **441**, 47.

23  V.P. Kandidov, O.G. Kosareva and A.A Koltun, Nonlinear-optical transformation of a high-power femtosecond laser pulse in air, *Quantum Electron.*, 2003, **33**, 69.

24  S.L. Chin, S.A. Hosseini, W. Liu, Q. Luo, F. Théberge, N. Aközbek, A. Becker, V.P. Kandidov, O.G. Kosareva and H. Schröder, The propagation of powerful femtosecond laser pulses in optical media: physics, applications, and new challenges, *Can. J. Phys.*, 2005, **83**, 863.

25  D.V. Apeksimov, O.A. Bukin, E.E. Bykova, Yu.E. Geints, S.S. Golik, A.A. Zemlyanov, A.A. Il'in, A.M. Kabanov, G.G. Matvienko, V.K. Oshlakov, A.V. Petrov and E.B. Sokolova, Filamentation of the focused Ti: Sapphire laser pulse in air at two harmonics, *Plasma Phys. Rep.*, 2013, **39**, 1074.

26  G. Mechain, C.D. Amico, Y.-B. Andre, S. Tzortzakis, M. Franco, B. Prade, A. Mysyrowicz, A. Couairon, E. Salmon and R. Sauerbrey, Range of plasma filaments created in air by a multi-terawatt femtosecond laser, *Opt. Commun.*, 2005, **247**, 171.

27  M. Durand, A. Houard, B. Prade, A. Mysyrowicz, A. Durécu, B. Moreau, D. Fleury, O. Vasseur, H. Borchert and K. Diener, Kilometer range filamentation, *Opt. Express*, 2013, **21**, 26836.

28  M. Rodriguez, R. Bourayou, G. Méjean, J. Kasparian, J. Yu, E. Salmon, A. Scholz, B. Stecklum, J. Eislöffel and U. Laux, Kilometer-range nonlinear propagation of femtosecond laser pulses, *Phys. Rev. E*, 2004, **69**, 036607.

29  A.A. Ionin, S.I. Kudryashov, S.V. Makarov, L.V. Seleznev and D.V. Sinitsyn, Multiple filamentation of intense femtosecond laser pulses in air, *JETP Lett.*, 2009, **90**, 423.

30  A.A. Ilyin and S.S. Golik, Absorption of laser-radiation energy by femtosecond laser spark in air, *Tech. Phys. Lett.*, 2014, **40**, 1.

31  W. Liu and S.L. Chin, Direct measurement of the critical power of femtosecond Ti : sapphire laser pulse in air, *Opt. Express*, 2005, **13**, 5750.

32  N. Zhang, W.-X. Bao, J.-H. Yang and X.-N. Zhu, Determination of the temporal structure of femtosecond laser pulses by means of laser-induced air plasma, *Chin. Phys. B*, 2013, **22**, 054209.

33  S. Xu, X. Sun, B. Zeng, W. Chu, J. Zhao, W. Liu, Y. Cheng, Z. Xu and S.L. Chin, Simple method of measuring laser peak intensity inside femtosecond laser filament in air, *Opt. Express*, 2012, **20**, 299.

34  K. Lim, M. Durand, M. Baudelet and M. Richardson, Transition from linear-to nonlinear-focusing regime in filamentation, *Sci. Rep.*, 2014, **4**, 7217.

35  P.P. Kiran, S. Bagchi, S.R. Krishnan, C.L. Arnold, G.R. Kumar and A. Couairon, Focal dynamics of multiple filaments: Microscopic imaging and reconstruction, *Phys. Rev. A*, 2010, **82**, 013805.

36  V.P. Kandidov, S.A. Shlenov, O.G. Kosareva, Filamentation of high-power femtosecond laser radiation, *Quantum Electron.*, 2009, **39**, 205.

37  A. Couairon and A. Mysyrowicz, in *Progress in Ultrafast Intense Laser Science*, ed. K. Yamanouchi, S. L. Chin, P. Agostini, G. Ferrante, Springer, 2006, vol. I, pp. 235-258.

38  F. Théberge, W. Liu, P.Tr. Simard, A. Becker and S.L. Chin, Plasma density inside a femtosecond laser filament in air: Strong dependence on external focusing, *Phys. Rev. E*, 2006, **74**, 036406.

39  J. Kasparian, R. Sauerbrey and S.L. Chin, The critical laser intensity of self-guided light filaments in air, *Appl. Phys. B*, 2000, **71**, 877.

40  N.B. Delone, *Basics of interaction of laser radiation with matter*, Editions Frontieres, 1993.

41  H.L. Xu, A. Azarm, J. Bernhardt, Y. Kamali and S.L. Chin, The mechanism of nitrogen fluorescence inside a femtosecond laser filament in air, *Chem. Phys.*, 2009, **360**, 171.

42  J.Yu, D. Mondelain, J. Kasparian, E. Salmon, S. Geffroy, C. Favre, V. Boutou and J.-P. Wolf, Sonographic probing of laser filaments in air, *Appl. Opt.*, 2003, **42**, 7117.

43  G.N. Gibson, R.R. Freeman and T.J. McIlrath, Dynamics of the high-intensity multiphoton ionization of $N_2$, *Phys. Rev. Lett.*, 1991, **67**, 1230.

44  Y.P. Raizer, *Laser-Induced Discharge Phenomena,* Consultants Bureau, 1977.

45  A.A. Ilyin, I.G. Nagorny and O.A. Bukin, Supersonic regimes of plasma expansion during optical breakdown in air, *Appl. Phys. Lett.*, 2010, **96**, 171501.

46  A.A. Ilyin, S.S. Golik and K.A. Shmirko, Absorption and emission characteristics of femtosecond laser plasma filaments in the air, *Spectrochim. Acta Part B*, 2015, **112**, 16.

47  F. Martin, R. Mawassi, F. Vidal, I. Gallimberti, D. Comtois, H. Pépin, J.C. Kieffer, and H.P. Mercure, Spectroscopic study of ultrashort pulse laser-breakdown plasmas in air, *Appl. Spectrosc.*, 2002, **56**, 1444.

48  S.L. Chin, H.L. Xu, Q. Luo, F. Théberge, W. Liu, J.F. Daigle, Y. Kamali, P.T. Simard, J. Bernhardt, S.A. Hosseini, M. Sharifi, G.

Méjean, A. Azarm, C. Marceau, O. Kosareva, V.P. Kandidov, N. Aközbek, A. Becker, G. Roy, P. Mathieu, J.R. Simard, M. Châteauneuf, and J. Dubois, Filamentation 'remote' sensing of chemical and biological agents/pollutants using only one femtosecond laser source, *Appl. Phys. B*, 2009, **95**, 1.

49  V. Zorba, X. Mao and R.E. Russo, Optical far- and near-field femtosecond laser ablation of Si for nanoscale chemical analysis, *Anal. Bioanal. Chem.*, 2010, **396**, 173.

50  S.-S. Wellershoff, J. Hohlfeld, J. Güdde and E. Matthias, The role of electron-phonon coupling in femtosecond laser damage of metals, *Appl. Phys. A*, 1999, **69**, S99.

51  F. Korte, S. Nolte, B.N. Chichkov, T.Bauer, G. Kamlage, T. Wagner, C. Fallnich and H. Welling, Far-field and near-field material processing with femtosecond laser pulses, *Appl. Phys. A*, 1999, **69**, S7.

52  E.G. Gamaly and A.V. Rode, Physics of ultra-short laser interaction with matter: From phonon excitation to ultimate transformations, *Prog. Quantum Electron.*, 2013, **37**, 215.

53  *Ultrafast Laser Processing: From Micro- to Nanoscale*, ed. K. Sugioka and Y. Cheng, Pan Stanford Publishing, 2013.

54  M. Lisowski, P.A. Loukakos, U. Bovensiepen, J. Stahler, C. Gahl and M. Wolf, Ultra-fast dynamics of electron thermalization, cooling and transport effects in Ru(001), *Appl. Phys. A*, 2004, **78**, 165.

55  N.M. Bulgakova, A.V. Bulgakov and O.F. Bobrenok, Double layer effects in laser-ablation plasma plumes, *Phys. Rev. E*, 2000, **62**, 5624.

56  A. Brantov, W. Rozmus, R. Sydora, C.E. Capjack, V.Yu. Bychenkov and V.T. Tikhonchuk, Enhanced inverse bremsstrahlung heating rates in a strong laser field, *Phys. Plasmas*, 2003, **10**, 3385.

57  W. Hu, Y.C. Shin and G. King, Energy transport analysis in ultrashort pulse laser ablation through combined molecular dynamics and Monte Carlo simulation, *Phys. Rev. B*, 2010, **82**, 094111.

58  N.M. Bulgakova, R. Stoian and A. Rosenfeld, Laser-induced modification of transparent crystals and glasses, *Quantum Electron.*, 2010, **40**, 966.

59  N.M. Bulgakova, V.P. Zhukov, A.Y. Vorobyev and C. Guo, Modeling of residual thermal effect in femtosecond laser ablation of metals: role of a gas environment, *Appl. Phys. A*, 2008, **92**, 883.

60  W. Hu, Y.C. Shin and G. King, Early-stage plasma dynamics with air ionization during ultrashort laser ablation of metal, *Phys. Plasmas*, 2011, **18**, 093302.

61  J. Li, X. Wang, Z. Chen, R. Clinite, S.S. Mao, P. Zhu, Z. Sheng, J. Zhang and J. Cao, Ultrafast electron beam imaging of femtosecond laser-induced plasma dynamics, *J. Appl. Phys.*, 2010, **107**, 083305.

ARTICLE

62  X. Zhao and Y.C. Shin, Coulomb explosion and early plasma generation during femtosecond laser ablation of silicon at high laser fluence, *J. Phys. D*, 2013, **46**, 335501.

63  X.-L. Liu, X. Lu, X. Liu, T.-T. Xi, F. Liu, J.-L. Ma and J. Zhang, Tightly focused femtosecond laser pulse in air: from filamentation to breakdown, *Opt. Express*, 2010, **18**, 26007.

64  A.E. Martirosyan, C. Altucci, A. Bruno, C. de Lisio, A. Porzio and S. Solimeno, Time evolution of plasma afterglow produced by femtosecond laser pulses, *J. Appl. Phys.*, 2004, **96**, 5450.

65  V.V. Bukin, N.S. Vorob'ev, S.V. Garnov, V.I. Konov, V.I. Lozovoi, A.A. Malyutin, M.Y. Shchelev and I.S. Yatskovskii, Formation and development dynamics of femtosecond laser microplasma in gases, *Quantum Electron.*, 2006, **36**, 638.

66  S.I. Anisimov, B.L. Kapeliovich and T.L. Perel'man, Electron-emission from surface of metals induced by ultrashort laser pulses, *Sov. Phys. JETP*, 1975, **39**, 375.

67  M.E. Povarnitsyn, T.E. Itina, M. Sentis, K.V. Khishchenko and P.R. Levashov, Material decomposition mechanisms in femtosecond laser interactions with metals, *Phys. Rev. B*, 2007, **23**, 235414.

68  B. Rethfeld, K. Sokolowski-Tinten, D. von der Linde and S.I. Anisimov, Timescales in the response of materials to femtosecond laser excitation, *Appl. Phys. A*, 2004, **79**, 767.

69  I. Mingareev, Ultrafast dynamics of melting and ablation at large laser intensities, PhD Thesis, RWTH- Aachen, 2009.

70  D.S. Ivanov and L.V. Zhigilei, Combined atomistic-continuum modeling of short-pulse laser melting and disintegration of metal films, *Phys. Rev. B*, 2003, **68**, 064114.

71  B. Rethfeld, K. Sokolowski-Tinten, D. von der Linde and S.I. Anisimov, Ultrafast thermal melting of laser-excited solids by homogeneous nucleation, *Phys. Rev. B*, 2002, **65**, 092103.

72  A. Rousse, C. Rischel, S. Fourmaux, I. Uschmann, S. Sebban, G. Grillon, P. Balcou, E. Förster, J.P. Geindre, P. Audebert, J. C. Gauthier and D. Hulin, Non-thermal melting in semiconductors measured at femtosecond resolution, *Nature*, 2001, **410**, 65.

73  J.P. Colombier, P. Combis, R. Stoian and E. Audouard, High shock release in ultrafast laser irradiated metals: Scenario for material ejection, *Phys. Rev. B*, 2007, **75**, 104105.

74  M.E. Povarnitsyn, K.V. Khishchenko, P.R. Levashov, Phase transitions in femtosecond laser ablation, *Appl. Surf. Sci.*, 2009, **255**, 5120.

75  A.A. Ionin, S.I. Kudryashov, L.V. Seleznev, D.V. Sinitsyn, A.F. Bunkin, V.N. Lednev and S.M. Pershin, Thermal melting and ablation of silicon by femtosecond laser radiation, *J. Exp. Theor. Phys.*, 2013, **116**, 347.

76  M.E. Povarnitsyn, T.E. Itina, P.R. Levashov and K.V. Khishchenko, Simulation of ultrashort double-pulse laser ablation, *Appl. Surf. Sci.*, 2011, **257**, 5168.

77  I. Mingareev and A. Horn, Time-resolved investigations of plasma and melt ejections in metals by pump-probe shadowgrpahy, *Appl. Phys. A*, 2008, **92**, 917.

78  O. Albert, S. Roger, Y. Glinec, J.C. Loulergue, J. Etchepare, C. Boulmer-Leborgne, J. Perriere and E. Millon, Time-resolved spectroscopy measurements of a titanium plasma induced by nanosecond and femtosecond lasers, *Appl. Phys. A*, 2003, **76**, 319.

79  D. Scuderi , R. Benzerga, O. Albert, B. Reynier and J. Etchepare, Spectral and temporal characteristics of metallic nanoparticles produced by femtosecond laser pulses, *Appl. Surf. Sci.*, 2006, **252**, 4360–4363.

80  S. Noël, J. Hermann and T. Itina, Investigation of nanoparticle generation during femtosecond laser ablation of metals, *Appl. Surf. Sci.*, 2007, **253**, 6310.

81  E. Axente, S. Noël, J. Hermann, M. Sentis and I.N. Mihailescu, Correlation between plasma expansion and damage threshold by femtosecond laser ablation of fused silica, *J. Phys. D*, 2008, **41**, 105216.

82  I. Mingareev and A. Horn, Melt dynamics of aluminum irradiated with ultrafast laser radiation at large intensities, *J. Appl. Phys.*, 2009, **106**, 013513.

83  N.M. Bulgakova and A.V. Bulgakov, Pulsed laser ablation of solids: transition from normal vaporization to phase explosion, *Appl. Phys. A*, 2001, **73**, 199.

84  A.A. Ilyin, I.G. Nagorny, O.A. Bukin, A.V. Bulanov and K.A. Shmirko, Features of development of optical breakdown on an inclined aluminum surface, *Tech. Phys. Lett.*, 2012, **38**, 975.

85  B.N. Chichkov, C. Momma, S. Nolte, F. yon Alvensleben and A. Tünnermann, Femtosecond, picosecond and nanosecond laser ablation of solids, *Appl. Phys. A*, 1996, **63**, 109.

86  M. Lopez-Claros, J.M. Vadillo and J.J. Laserna, Determination of plasma ignition threshold fluence during femtosecond single-shot laser ablation on metallic samples detected by optical emission spectroscopy, *J. Anal. At. Spectrom.*, 2015, **30**, 1730.

87  S. Hofmann, Quantitative Depth Profiling in Surface Analysis: A Review, *Surf. Interface Anal.*, 1980, **2**, 148.

88  Compendium of Analytical Nomenclature: Orange Book of IUPAC. Definitive Rules; 1997. Part 17.4 Terms related to surface analysis.

89  V. Margetic, M. Bolshov, A. Stockhaus, K. Niemax and R. Hergenröder, Depth profiling of multi-layer samples using femtosecond laser ablation, *J. Anal. At. Spectrom.*, 2001, **16**, 616.

90  A. Baskevicius, A. Alesenkov, G. Chozevskis, J. Litvaityte, O. Balachninaite, D. Paipulas, A. Melninkaitis and V. Sirutkaitis, Optimization of Laser-Ablation Micromachining by Choice of

Scanning Algorithms and Use of Laser-Induced-Breakdown Spectroscopy, *J. Laser Micro/Nanoeng.*, 2013, **8**, 24.

91 O. Samek, V. Hommes, R. Hergenröder and S.V. Kukhlevsky, Femtosecond pulse shaping using a liquid–crystal display: Applications to depth profiling analysis, *Rev. Sci. Instrum.*, 2005, **76**, 086104.

92 S.P. Banerjee, Z. Chen, I. Utkin and R. Fedosejevs, Detection of buried layers in silicon devices using LIBS during hole drilling with femtosecond laser pulses, *Appl. Phys. A*, 2013, **111**, 791.

93 D. McGloin and K. Dholakia, Bessel beams: diffraction in a new light, *Contemp. Phys.*, 2005, **46**, 15.

94 J. Durnin, J.J. Miceli, Jr., and J.H. Eberly, Diffraction-free beams, *Phys. Rev. Lett.*, 1987, **58**, 1499.

95 J. Arlt and K. Dholakia, Generation of high-order Bessel beams by use of an axicon, *Opt. Commun.*, 2000, **177**, 297.

96 F. Courvoisier, J. Zhang, M.K. Bhuyan, M. Jacquot and·J.M. Dudley, Applications of femtosecond Bessel beams to laser ablation, *Appl. Phys. A*, 2013, **112**, 29.

97 D.E. Roberts, A. du Plessis, J. Steyn, L.R. Botha, C.A. Strydom, I.J. van Rooyen, Femtosecond laser induced breakdown spectroscopy of silver within surrogate high temperature gas reactor fuel coated particles, *Spectrochim. Acta Part B*, 2010, **65**, 918.

98 S.P. Banerjee and R. Fedosejevs, Single shot depth sensitivity using femtosecond Laser Induced Breakdown Spectroscopy, *Spectrochim. Acta Part B*, 2014, **92**, 34.

99 P. Pouli, K. Melessanaki, A. Giakoumaki, V. Argyropoulos and D. Anglos, Measuring the thickness of protective coatings on historic metal objects using nanosecond and femtosecond laser induced breakdown spectroscopy depth profiling, *Spectrochim. Acta Part B*, 2005, **60**, 1163.

100 A. De Bonis, B. De Filippo, A. Galasso, A. Santagata, A. Smaldone and R. Teghil, Comparison of the performances of nanosecond and femtosecond Laser Induced Breakdown Spectroscopy for depth profiling of an artificially corroded bronze, *Appl. Surf. Sci.*, 2014, **302**, 275.

101 D.W. Hahn and N. Omenetto, Laser-Induced Breakdown Spectroscopy (LIBS), Part II: Review of Instrumental and Methodological Approaches to Material Analysis and Applications to Different Fields, *Appl. Spectrosc.*, 2012, **66**, 347.

102 C. Liu, X.L. Mao, S.S. Mao, X. Zeng, R. Greif and R.E. Russo, Nanosecond and Femtosecond Laser Ablation of Brass: Particulate and ICPMS Measurements, *Anal. Chem.*, 2004, **76**, 379.

103 C. Jeynes, N.P. Barradas and E. Szilagyi, Accurate Determination of Quantity of Material in Thin Films by Rutherford Backscattering Spectrometry, *Anal. Chem.*, 2012, **84**, 6061.

104 A.H. Galmed, A.K. Kassem, H. Von Bergmann and M.A. Harith, A study of using femtosecond LIBS in analyzing metallic thin film–semiconductor interface, *Appl. Phys. B*, 2011, **102**, 197.

105 D.K. Das, J.P. McDonald, S.M. Yalisove and T.M. Pollock, Depth-profiling study of a thermal barrier coated superalloy using femtosecond laser-induced breakdown spectroscopy, *Spectrochim. Acta Part B*, 2008, **63**, 27.

106 C.C. García, M. Corral, J.M. Vadillo and J.J. Laserna, Angle-resolved laser-induced breakdown spectrometry for depth profiling of coated materials, *Appl. Spectrosc.*, 2000, **54**, 1027.

107 T. Kratochvíl, T. Černohorský, P. Knotek, L. Kalina, J. Návesník, M. Pouzar and M. Zvolská, Fast determination of the surface density of titanium in ultrathin layers using LIBS spectrometry, *J. Anal. At. Spectrom.*, 2014, **29**, 1806.

108 A. Assion, M. Wollenhaupt, L. Hag, F. Mayorov, C. Sarpe-Tudoran, M. Winter, U. Kutschera and T. Baumert, Femtosecond laser-induced-breakdown spectrometry for $Ca^{2+}$ analysis of biological samples with high spatial resolution, *Appl. Phys. B*, 2003, **77**, 391.

109 O. Samek, J. Lambert, R. Hergenröder, M. Liška, J. Kaiser, K. Novotný and S. Kukhlevsky, Femtosecond laser spectrochemical analysis of plant samples, *Laser Phys. Lett.*, 2006, **3**, 21.

110 J. Kaiser, O. Samek, L. Reale, M. Liška, R. Malina, A. Ritucci, A. Poma, A. Tucci, F. Flora, A. Lai, L. Mancini, G. Tromba, F. Zanini, A. Faenov, T. Pikuz and G. Cinque, Monitoring of the Heavy-Metal Hyperaccumulation in Vegetal Tissues by X-ray Radiography and by Femto-Second Laser Induced Breakdown Spectroscopy, *Microsc. Res. Tech.*, 2007, **70**, 147.

111 M.T. Taschuk, Y.Y. Tsui and R. Fedosejevs, Detection and Mapping of Latent Fingerprints by Laser-Induced Breakdown Spectroscopy, *Appl. Spectrosc.*, 2006, **60**, 1322.

112 S.P. Banerjee, Z. Chen and R. Fedosejevs, High resolution scanning microanalysis on material surfaces using UV femtosecond laser induced breakdown spectroscopy, *Opt. Lasers Eng.*, 2015, **68**, 1.

113 I.V. Cravetchi, M.T. Taschuk, Y.Y. Tsui and R. Fedosejevs, Evaluation of femtosecond LIBS for spectrochemical microanalysis of aluminium alloys, *Anal. Bioanal. Chem.*, 2006, **385**, 287.

114 T. Tong, J. Li and J.P. Longtin, Real-time control of ultrafast laser micromachining by laser-induced breakdown spectroscopy, *Appl. Optics*, 2004, **43**, 1971.

115 W. Wessel, A. Brueckner-Foit, J. Mildner, L. Englert, L. Haag, A. Horn, M. Wollenhaupt and T. Baumert, Use of femtosecond laser-induced breakdown spectroscopy (fs-LIBS) for micro-crack analysis on the surface, *Eng. Fract. Mech.*, 2010, **77**, 1874.

116 H. Hou, L. Cheng, T. Richardson, G. Chen, M. Doeff, R. Zheng, R.E. Russo, and V. Zorba, Three-Dimensional Elemental Imaging of Li-ion Solid-State Electrolytes Using fs-Laser Induced Breakdown Spectroscopy (LIBS), *J. Anal. At. Spectrom.*, 2015, DOI: 10.1039/C5JA00250H.

Journal Name

ARTICLE

117    M. Duocastella and C.B. Arnold, Bessel and annular beams for materials processing, *Laser Photonics Rev.*, 2012, **6**, 607.

118    Q. Zhan, Cylindrical vector beams: from mathematical concepts to applications, *Adv. Opt. Photonics*, 2009, **1**, 1.

119    C. Hnatovsky, V. Shvedov, W. Krolikowski and A. Rode, Revealing Local Field Structure of Focused Ultrashort Pulses, *Phys. Rev. Lett.*, 2011, **106**, 123901.

120    E. Betzig and J.K. Trautman, Near-Field Optics: Microscopy, Spectroscopy, and Surface Modification Beyond the Diffraction Limit, *Science*, 1992, **257**, 189.

121    V. Zorba, X. Mao and R.E. Russo, Ultrafast laser induced breakdown spectroscopy for high spatial resolution chemical analysis, *Spectrochim. Acta Part B*, 2011, **66**, 189.

122    R.E. Russo, T.W. Suen, A.A. Bol'shakov, J. Yoo, O. Sorkhabi, X. Mao, J. Gonzalez, D. Oropeza and V. Zorba, Laser plasma spectrochemistry, *J. Anal. At. Spectrom.*, 2011, **26**, 1596.

123    Y. Lu, V. Zorba, X. Mao, R. Zheng and R.E. Russo, UV fs–ns double-pulse laser induced breakdown spectroscopy for high spatial resolution chemical analysis, *J. Anal. At. Spectrom.*, 2013, **28**, 743.

124.    G.W. Rieger, M. Taschuk, Y.Y. Tsui and R. Fedosejevs, Comparative study of laser-induced plasma emission from microjoule picosecond and nanosecond KrF-laser pulses, *Spectrochim. Acta Part B*, 2003, **58**, 497.

125    B. Le Drogoff, M. Chaker, J. Margot, M. Sabsabi, O. Barthélemy, T. W. Johnston, S. Laville and F. Vidal, Influence of the Laser Pulse Duration on Spectrochemical Analysis of Solids by Laser-Induced Plasma Spectroscopy, *Appl. Spectrosc.*, 2004, **58**, 122.

126    T. Gunaratne, M. Kangas, S. Singh, A. Gross and M. Dantus, Influence of bandwidth and phase shaping on laser induced breakdown spectroscopy with ultrashort laser pulses, *Chem. Phys. Lett.*, 2006, **423**, 197.

127    V. Piñon and D. Anglos, Optical emission studies of plasma induced by single and double femtosecond laser pulses, *Spectrochim. Acta Part B*, 2009, **64**, 950.

128    E. Tognoni, V. Palleschi, M. Corsi and G. Cristoforetti, Quantitative micro-analysis by laser-induced breakdown spectroscopy: a review of the experimental approaches, *Spectrochim. Acta Part B*, 2002, **57**, 1115.

129    J.T. Schiffern, D.W. Doerr and D.R. Alexander, Optimization of collinear double-pulse femtosecond laser-induced breakdown spectroscopy of silicon, *Spectrochim. Acta Part B*, 2007, **62**, 1412.

130    D. Santos, R.E. Samad, L.C. Trevizan, A.Z. de Freitas, N.D. Vieira and F.J. Krug, Evaluation of Femtosecond Laser-Induced Breakdown Spectroscopy for Analysis of Animal Tissues, *Appl. Spectrosc.*, 2008, **62**, 1137.

131    J. Scaffidi, W. Pearman, J.C. Carter and S.M. Angel, Observations in collinear femtosecond–nanosecond dual-pulse laser-induced breakdown spectroscopy, *Appl. Spectrosc.*, 2006, **60**, 65.

132    Ş. Yalçin, Y.Y. Tsui and R. Fedosejevs, Pressure dependence of emission intensity in femtosecond laser-induced breakdown spectroscopy, *J. Anal. At. Spectrom.*, 2004, **19**, 1295.

133    L.A. Emmert, R.C. Chinni, D.A. Cremers, C.R. Jones and W. Rudolph, Comparative study of femtosecond and nanosecond laser-induced breakdown spectroscopy of depleted uranium, *Appl. Opt.*, 2011, **50**, 313.

134    A.W. Schill, D.A. Heaps, D.N. Stratis-Cullum, B.R. Arnold, P.M. Pellegrino, Characterization of near-infrared low energy ultra-short laser pulses for portable applications of laser induced breakdown spectroscopy, *Opt. Express*, 2007, **15**, 14044.

135    C.A. Zuhlke, J. Bruce III, T.P. Anderson, D.R. Alexander and C.G. Parigger, A Fundamental Understanding of the Dependence of the Laser-Induced Breakdown Spectroscopy (LIBS) Signal Strength on the Complex Focusing Dynamics of Femtosecond Laser Pulses on Either Side of the Focus, *Appl. Spectrosc.*, 2014, **68**, 1021.

136    M.P. Mateo, V. Piñon, D. Anglos and G. Nicolas, Effect of ambient conditions on ultraviolet femtosecond pulse laser induced breakdown spectra, *Spectrochim. Acta Part B*, 2012, **74-75**, 18.

137    A. Nakimana, H. Tao, X. Gao, Z. Hao and J. Lin, Effects of ambient conditions on femtosecond laser-induced breakdown spectroscopy of Al, *J. Phys. D*, 2013, **46**, 285204.

138 S.S. Harilal, N. Farid, J.R. Freeman, P.K. Diwakar, N.L. LaHaye and A. Hassanein, Background gas collisional effects on expanding fs and ns laser ablation plumes, *Appl. Phys. A*, 2014, **117**, 319.

139    N. Smijesh and R. Philip, Emission dynamics of an expanding ultrafast-laser produced Zn plasma under different ambient pressures, *J. Appl. Phys.*, 2013, **114**, 093301.

140    M. Guillermin, C. Liebig, F. Garrelie, R. Stoian, A.-S. Loir and E. Audouard, Adaptive control of femtosecond laser ablation plasma emission, *Appl. Surf. Sci.*, 2009, **255**, 5163.

141    M. Guillermin, J.P. Colombier, S. Valette, E. Audouard, F. Garrelie and R. Stoian, Optical emission and nanoparticle generation in Al plasmas using ultrashort laser pulses temporally optimized by real-time spectroscopic feedback, *Phys. Rev B*, 2010, **82**, 035430.

142    M. Guillermin, A. Klini, J.P. Colombier, F. Garrelie, D. Gray, C.Liebig, E. Audouard, C. Fotakis and R. Stoian, Tuning spectral properties of ultrafast laser ablation plasmas from brass using adaptive temporal pulse shaping, *Opt. Express*, 2010, **18**, 11159.

143    K.C. Hartig, J.P. McNutt, P. Ko, T.W. Jacomb-Hood and I. Jovanovic, Pulse chirp effects in ultrafast laser-induced breakdown spectroscopy, *J. Radioanal. Nucl. Chem.*, 2013, **296**, 135.

144    S.M. Angel, D.N. Stratis, K.L. Eland, T. Lai, M.A. Berg and D.M. Gold, LIBS using dual- and ultra-short laser pulses, *Fres. J Anal. Chem.*, 2001, **369**, 320.

145    B. Le Drogoff, J. Margot, F. Vidal, S. Laville, M. Chaker, M. Sabsabi, T.W. Johnston and O. Barthélemy, Influence of the laser pulse duration on laser-produced plasma properties, *Plasma Sources Sci. Technol.*, 2004, **13**, 223.

146    J.R. Freeman, S.S. Harilal, P.K. Diwakar, B. Verhoff and A. Hassanein, Comparison of optical emission from nanosecond and femtosecond laser produced plasma in atmosphere and vacuum conditions, *Spectrochim. Acta Part B*, 2013, **87**, 43.

147    Y. Liu, S. Singha, T.E. Witt, Y. Cheng and R.J. Gordon, Observation of near total polarization in the ultrafast laser ablation of Si, *Appl. Phys. Lett.*, 2008, **93**, 161502.

148    J.S. Penczak, Y. Liu and R.J. Gordon, Polarization Resolved Laser-Induced Breakdown Spectroscopy of Al, *J. Phys. Chem. A*, 2009, **113**, 13310.

149    Y. Zhao, S. Singha, Y. Liu and R.J. Gordon, Polarization-resolved laser-induced breakdown spectroscopy, *Opt. Lett.*, 2009, **34**, 494.

150    J.S. Penczak, Y. Liu, R.D. Schaller, D.H. Rich and R.J. Gordon, The mechanism for continuum polarization in laser induced breakdown spectroscopy of Si(111), *Spectrochim. Acta Part B*, 2012, **74-75**, 3.

151    J. Serrano, J. Moros and J.J. Laserna, Exploring the Formation Routes of Diatomic Hydrogenated Radicals Using Femtosecond Laser-Induced Breakdown Spectroscopy of Deuterated Molecular Solids, *J. Anal. At. Spectrom.*, 2015, DOI: 10.1039/C5JA00192G.

152    Y. Dikmelik and J.B. Spicer, Femtosecond laser-induced breakdown spectroscopy of explosives and explosive-related compounds, *Proc. SPIE*, 2005, **5794**, 757.

153    Y. Dikmelik, C. McEnnis and J.B. Spicer, Femtosecond and nanosecond laser-induced breakdown spectroscopy of trinitrotoluene, *Opt. Express*, 2008, **16**, 5332.

154    F.C. De Lucia Jr., J.L. Gottfried and A.W. Miziolek, Evaluation of femtosecond laser-induced breakdown spectroscopy for explosive residue detection, *Opt. Express*, 2009, **17**, 419.

155    S. Sunku, M.K. Gundawar, A.K. Myakalwar, P.P. Kiran, S.P. Tewari and S.V. Rao, Femtosecond and nanosecond laser induced breakdown spectroscopic studies of NTO, HMX, and RDX, *Spectrochim. Acta Part B*, 2013, **79–80**, 31.

156    S. Sunku, E.N. Rao, G.M. Kumar, S.P. Tewari and S.V. Rao, Molecular formation dynamics of 5-nitro-2,4-dihydro-3H-1,2, 4-triazol-3-one,1,3,5-trinitroperhydro-1,3,5-triazine,     and 2,4,6-trinitrotoluene in air, nitrogen, and argon atmospheres studied using femtosecond laser induced breakdown spectroscopy, *Spectrochim. Acta Part B*, 2013, **87**, 121.

157    B. Yee, K.C. Hartig, P. Ko, J. McNutt and I. Jovanovic, Measurement of boron isotopic ratio with non-gated molecular spectroscopy of femtosecond laser-produced plasma, *Spectrochim. Acta Part B*, 2013, **79–80**, 72.

158    H. Hou, G.C.-Y. Chan, X. Mao, V. Zorba, R. Zheng and R.E. Russo, Femtosecond Laser Ablation Molecular Isotopic Spectrometry for Zirconium Isotope Analysis, *Anal. Chem.*, 2015, **87**, 4788.

159    H. Hou, G.C.-Y. Chan, X. Mao, R. Zheng, V. Zorba and R.E. Russo, Femtosecond filament-laser ablation molecular isotopic spectrometry, *Spectrochim. Acta Part B*, 2015, **113**, 113.

160    V.I. Babushok, F.C. De Lucia jr, J.L. Gottfried, C.A. Munson and A.W. Miziolek, Double pulse laser ablation and plasma: Laser induced breakdown spectroscopy signal enhancement, *Spectrochim. Acta Part B*, 2006, **61**, 999.

161    E. Tognoni and G. Cristoforetti, Basic mechanisms of signal enhancement in ns double-pulse laser-induced breakdown spectroscopy in a gas environment, *J. Anal. At. Spectrom.*, 2014, **29**, 1318.

162    A. Santagata, R. Teghil, G. Albano, D. Spera, P. Villani , A. De Bonis, G.P. Parisi and A. Galasso, fs/ns dual-pulse LIBS analytic survey for copper-based alloys, *Appl. Surf. Sci.*, 2007, **254**, 863.

163    M.E. Povarnitsyn, T.E. Itina, K.V. Khishchenko and P.R. Levashov, Suppression of Ablation in Femtosecond Double-Pulse Experiments, *Phys. Rev. Lett.*, 2009, **103**, 195002.

164    S. Noël, E. Axente and J. Hermann, Investigation of plumes produced by material ablation with two time-delayed femtosecond laser pulses, *Appl. Surf. Sci.*, 2009, **255**, 9738.

165    R. Teghil, A. Santagata, A. De Bonis, G. Albano, P. Villani, D. Spera, G.P. Parisi and A. Galasso, Applications of ultra-short pulsed laser ablation: thin films deposition and fs/ns dual-pulse laser-induced breakdown spectroscopy, *Phys. Scr.*, 2008, **78**, 058113.

166    A. Santagata, G. Albano, D. Spera, R. Teghil, P. Villani, G.P. Parisi, A. De Bonis and D.J. Sordelet, Emission spectra investigation of fs induced NPs probed by the ns laser pulse of a fs/ns DP-LIBS orthogonal configuration, *Appl. Surf. Sci.*, 2009, **255**, 5159.

167    J. Hermann, L. Mercadier, E. Axente and S. Noël, Properties of plasmas produced by short double pulse laser ablation of metals, *J. Phys. Conf. Ser.*, 2012, **399**, 012006.

168    A. Guarnaccio, G.P. Parisi, D.Mollica, A. De Bonis, R. Teghil and A. Santagata, Fs–ns double-pulse Laser Induced Breakdown Spectroscopy of copper-based-alloys: Generation and elemental analysis of nanoparticles, *Spectrochim. Acta Part B*, 2014, **101**, 261.

169    A. Semerok, C. Chaléard, V. Detalle, J.-L. Lacour, P. Mauchien, P. Meynadieκ, C. Nouvellon, B. Sallé, P. Palianov, M. Perdrix and G. Petite, Experimental investigations of laser ablation efficiency of pure metals with femto, pico and nanosecond pulses, *Appl. Surf. Sci.*, 1999, **138–139**, 311.

170    B. Le Drogoff, J. Margot, M. Chaker, M. Sabsabi, O. Barthélemy, T.W. Johnston, S. Laville, F. Vidal and Y. von Kaenel, Temporal characterization of femtosecond laser

Journal Name

ARTICLE

pulses induced plasma for spectrochemical analysis of aluminum alloys, *Spectrochim. Acta Part B*, 2001, **56**, 987.

171    A. Elhassan, A. Giakoumaki, D. Anglos, G.M. Ingo, L. Robbiola and M.A. Harith, Nanosecond and femtosecond Laser Induced Breakdown Spectroscopic analysis of bronze alloys, *Spectrochim. Acta Part B*, 2008, **63**, 504.

172    L. Fornarini, R. Fantoni, F. Colao, A. Santagata, R. Teghil, A. Elhassan and M.A. Harith, Theoretical Modeling of Laser Ablation of Quaternary Bronze Alloys: Case Studies Comparing Femtosecond and Nanosecond LIBS Experimental Data, *J. Phys. Chem. A*, 2009, **113**, 14364.

173    J. Scaffidi, J. Pender, W. Pearman, S.R. Goode, B.W. Colston Jr., J.C. Carter and S.M. Angel, Dual-pulse laser-induced breakdown spectroscopy with combinations of femtosecond and nanosecond laser pulses, *Appl. Opt.*, 2003, **42**, 6099.

174    J. Scaffidi, W. Pearman, M. Lawrence, J.C. Carter, B.W. Colston Jr. and S.M. Angel, Spatial and temporal dependence of interspark interactions in femtosecond–nanosecond dual-pulse laser-induced breakdown spectroscopy, *Appl. Opt.*, 2004, **43**, 5243.

175    J. Scaffidi, W. Pearman, J.C. Carter, B.W. Colston Jr. and S.M. Angel, Temporal dependence of the enhancement of material removal in femtosecond–nanosecond dual-pulse laser-induced breakdown spectroscopy, *Appl. Opt.*, 2004, **43**, 6492.

176    D. Scuderi, O. Albert, D. Moreau, P.P. Pronko and J. Etchepare, Interaction of a laser-produced plume with a second time delayed femtosecond pulse, *Appl. Phys. Lett.*, 2005, **86**, 071502.

177    A. Santagata, A. De Bonis, P. Villani, R. Teghil and G.P. Parisi, Fs/ns-dual-pulse orthogonal geometry plasma plume reheating for copper-based-alloys analysis, *Appl. Surf. Sci.*, 2006, **252**, 4685.

178    A. Santagata, R. Teghil, A. De Giacomo, M. Dell'Aglio, G.P. Parisi, A. De Bonis and A. Galasso, Optical emission spectroscopy investigation of an ultra-short laser induced titanium plasma reheated by a ns laser pulse, *Appl. Surf. Sci.*, 2007, **253**, 7792.

179    J.P. McDonald, D.K. Das, J.A. Nees, T.M. Pollock and S.M. Yalisove, Approaching non-destructive surface chemical analysis of CMSX-4 superalloy with double-pulsed laser induced breakdown spectroscopy, *Spectrochim. Acta Part B*, 2008, **63**, 561.

180    V. Piñon, C. Fotakis, G. Nicolas and D. Anglos, Double pulse laser-induced breakdown spectroscopy with femtosecond laser pulses, *Spectrochim. Acta Part B*, 2008, **63**, 1006.

181    V. Piñón, D. Anglos and G. Nicolás, Improvement of laser induced breakdown spectroscopy technique using double pulse schemes, *Ópt. Pura Apl.*, 2010, **43**, 113.

182    S. Singha, Z. Hu and R.J. Gordon, Ablation and plasma emission produced by dual femtosecond laser pulses, *J. Appl. Phys.*, 2008, **104**, 113520.

183    S. Amoruso, R. Bruzzese and X. Wang, Plume composition control in double pulse ultrafast laser ablation of metals, *Appl. Phys. Lett.*, 2009, **95**, 251501.

184    S. Amoruso, R. Bruzzese, X. Wang, G. O'Connell and J.G. Lunney, Multidiagnostic analysis of ultrafast laser ablation of metals with pulse pair irradiation, *J. Appl. Phys.*, 2010, **108**, 113302.

185    S. Noël and J. Hermann, Reducing nanoparticles in metal ablation plumes produced by two delayed short laser pulses, *Appl. Phys. Lett.*, 2009, **94**, 053120.

186    O. Balachninaitė, A. Baškevičius, K. Stankevičiūtė, K. Kuršelis and V. Sirutkaitis, Double-pulse laser-induced breakdown spectroscopy with 1030 and 257.5 nm wavelength femtosecond laser pulses, *Lithuan. J. Phys.*, 2010, **50**, 105.

187    M. Oba, Y. Maruyama, K. Akaoka, M. Miyabe and I. Wakaida, Double-pulse LIBS of gadolinium oxide ablated by femto- and nano-second laser pulses, *Appl. Phys. A*, 2010, **101**, 545.

188    F. Bourquard, J.-P. Colombier, M. Guillermin, A.-S. Loir, C. Donnet, R. Stoian and F. Garrelie, Temporal pulse shaping effects on aluminium and boron ablation plumes generated by ultrashort pulsed laser ablation and analyzed by time- and space-resolved optical spectroscopy, *Appl. Surf. Sci.*, 2012, **258**, 9374.

189    J. Guo, T. Wang, J. Shao, T. Sun, R. Wang, A. Chen, Z. Hu, M. Jin and D. Ding, Emission enhancement ratio of the metal irradiated by femtosecond double-pulse laser, *Opt. Comm.*, 2012, **285**, 1895.

190    A. Chen, S. Li, S. Li, Y. Jiang, J. Shao, T. Wang, X. Huang, M. Jin and D. Ding, Optimally enhanced optical emission in laser-induced air plasma by femtosecond double-pulse, *Phys. Plasmas*, 2013, **20**, 103110.

191    S.S. Harilal, P.K. Diwakar and A. Hassanein, Electron-ion relaxation time dependent signal enhancement in ultrafast double-pulse laser-induced breakdown spectroscopy, *Appl. Phys. Lett.*, 2013, **103**, 041102.

192    J. Penczak, R. Kupfer, I. Bar and R.J. Gordon, The role of plasma shielding in collinear double-pulse femtosecond laser-induced breakdown spectroscopy, *Spectrochim. Acta Part B*, 2014, **97**, 34.

193    J. Mildner, C. Sarpe, N. Götte, M. Wollenhaupt and T. Baumert, Emission signal enhancement of laser ablation of metals (aluminumand titanium) by time delayed femtosecond double pulses from femtoseconds to nanoseconds, *Appl. Surf. Sci.*, 2014, **302**, 291.

194    A. Semerok and C. Dutouquet, Analytical performances of laser-induced micro-plasma of Al samples with single and double ultrashort pulses in air and with Ar-jet: A comparative study, *Spectrochim. Acta Part B*, 2014, **99**, 163.

195    X. Liu, S. Sun, X. Wang, Z. Liu, Q. Liu, P. Ding, Z. Guo and B. Hu, Effect of laser pulse energy on orthogonal double femtosecond pulse laser-induced breakdown spectroscopy, *Opt. Express*, 2013, **21**, A704.

196    H. Qi, S. Li, Y. Qi, A. Chen, Z. Hu, X. Huang, M. Jin and D. Ding, Effect of sample position on collinear femtosecond double-pulse laser-induced breakdown spectroscopy of silicon in air, *J. Anal. At. Spectrom.*, 2014, **29**, 1105.

197    Y. Qi, H. Qi, Q. Wang, Z. Chen and Z. Hun, The influence of double pulse delay and ambient pressure on femtosecond laser ablation of silicon, *Opt. Laser Technol.*, 2015, **66**, 68.

198    X. Zhao and Y.C. Shin, Laser–plasma interaction and plasma enhancement by ultrashort double‑pulse ablation, *Appl. Phys. B*, 2015, **120**, 81.

199    J. Shen, Z. Yang, X. Liu, Y. Shi, P Zhao, S. Sun and B. Hu, Analysis of Enhanced Laser-Induced Breakdown Spectroscopy with Double Femtosecond Laser Pulses, *Plasma Sci. Technol.*, 2015, **17**, 147.

200    M. Wang, S. Wang, Z. Cao, P. Wang and C. Wang, Investigation of double-pulse femtosecond laser induced breakdown spectroscopy of polymethyl methacrylate (PMMA), *Proc. SPIE*, 2015, **9351**, 93511Q.

201    J.J. Laserna, R. Fernández Reyes, R. González, L. Tobaria and P. Lucena, Study on the effect of beam propagation through atmospheric turbulence on standoff nanosecond laser induced breakdown spectroscopy measurements, *Opt. Express*, 2009, **17**, 10265.

202    P. Rohwetter, J. Yu, G. Mejean, K. Stelmaszczyk, E. Salmon, J. Kasparian, J.-P. Wolf and L. Woste, Remote LIBS with ultrashort pulses: characteristics in picosecond and femtosecond, *J. Anal. At. Spectrom.*, 2004, **19**, 437.

203    K.Y. Andrianov, V.P. Kandidov, O.G. Kosareva, S.L. Chin, A. Talebpur, S. Petit, W. Liu, A. Ivasaki and M.C. Nadeau, Influence of beam quality on filamentation of high-power femtosecond laser pulses in air, *Izv. Akad. Nauk Ser. Fiz.*, 2002, **66**, 1091.

204    V.P. Kandidov, O.G. Kosareva, S.A. Shlenov, N.A. Panov, V.Y. Fedorov and A.E. Dormidonov, Dynamic small-scale self-focusing of a femtosecond laser pulse, *Quantum Electron.*, 2005, **35**, 59.

205    K. Stelmaszczyk, P. Rohwetter, G. Mejean, J. Yu, E. Salmon, J. Kasparian, R. Ackermann, J.P. Wolf and L. Woste, Long-distance remote laser-induced breakdown spectroscopy using filamentation in air, *Appl. Phys. Lett.*, 2004, **85**, 3977.

206    H. Wille, M. Rodriguez, J. Kasparian, D. Mondelain, J. Yu, A. Mysyrowicz, R. Sauerbrey, J.P. Wolf and L. Woste, Teramobile: A mobile femtosecond-terawatt laser and detection system, *Eur. Phys. J.*, 2002, **20**, 183.

207    R.S. Hatzes, Kilometer-range non-linear propagation of fs laser pulses, *Phys. Rev. E*, 2004, **69**, 036607.

208    C. D'Amico, A. Houard, M. Franco, B. Prade and A. Mysyrowicz, Coherent and incoherent radial THz radiation emission from femtosecond filaments in air, *Opt. Express*, 2007, **15**, 15274.

209    G. Méchain, T. Olivier, M. Franco, A. Couairon, B. Prade and A. Mysyrowicz, Femtosecond filamentation in air at low pressures. Part II: Laboratory experiments, *Opt. Commun.*, 2006, **261**, 322.

210    J. Kasparian, R. Ackermann, Y.-B. Andre, G. Mechain, G. Mejean, B. Prade, P. Rohwetter, E. Salmon, K. Stelmaszczyk, J. Yu, A. Mysyrowicz, R. Sauerbrey, L. Woste and J.-P. Wolf, Progress towards lightning control using lasers, *J. Eur. Opt. Soc. Rapid Publ.*, 2008, **3**, DOI: 10.2971/jeos.2008.08035.

211    Y. Petit, S. Henin, J. Kasparian, J.-P. Wolf, P. Rohwetter, K. Stelmaszczyk, Z. Q. Hao, W. M. Nakaema, L. Wöste and A. Vogel, Influence of pulse duration, energy, and focusing on laser-assisted water condensation, *Appl. Phys. Lett.*, 2011, **98**, 041105.

212    http://www.teramobile.org

213    P. Rohwetter, K. Stelmaszczyk, L. Wöste, R. Ackermann, G. Méjean, E. Salmon, J. Kasparian, J. Yu and J.-P. Wolf, Filament-induced remote surface ablation for long range laser-induced breakdown spectroscopy operation, *Spectrochim. Acta Part B*, 2005, **60**, 1025.

214    M. Weidman, K. Lim, M. Ramme, M. Durand, M. Baudelet and M. Richardson, Stand-off filament-induced ablation of gallium arsenide, *Appl. Phys. Lett.*, 2012, **101**, 034101.

215    A. Valenzuela, C. Munson, A. Porwitzky, M. Weidman and M. Richardson, Comparison between geometrically focused pulses versus filaments in femtosecond laser ablation of steel and titanium alloys, *Appl. Phys. B*, 2014, **116**, 485.

216    M. Weidman, M. Baudelet, M. Fisher, C. Bridge, C. Brown, M. Sigman, P.J. Dagdigian and M. Richardson, Molecular signal as a signature for detection of energetic materials in filament-induced breakdown spectroscopy, *Proc. SPIE*, 2009, **7304**, 73041G-1.

217    W. Liu, H.L. Xu, G. Méjean, Y. Kamali, J.-F. Daigle, A. Azarm, P.T. Simard, P. Mathieu, G. Roy and S.L. Chin, Efficient non-gated remote filament-induced breakdown spectroscopy of metallic sample, *Spectrochim. Acta Part B*, 2007, **62**, 76.

218    H.L. Xu, J. Bernhardt, P. Mathieu, G. Roy and S.L. Chin, Understanding the advantage of remote femtosecond laser-induced breakdown spectroscopy of metallic targets, *J. Appl. Phys.*, 2007, **101**, 033124.

219    E.J. Judge, G. Heck, E.B. Cerkez and R.J. Levis, Discrimination of Composite Graphite Samples Using Remote Filament-Induced Breakdown Spectroscopy, *Anal. Chem.*, 2009, **81**, 2658.

220    H.L. Xu, P.T. Simard, Y. Kamali, J.-F. Daigle, C. Marceau, J. Bernhardt, J. Dubois, M. Châteauneuf, F. Théberge and G. Roy, Filament-induced breakdown remote spectroscopy in a polar environment, *Laser Phys.*, 2012, **22**, 1767.

221    S. Tzortzakis, D. Anglos and D. Gray, Ultraviolet laser filaments for remote laser-induced breakdown spectroscopy (LIBS) analysis: applications in cultural heritage monitoring, *Opt. Lett.*, 2006, **31**, 1139.

222    D. Mirell, O. Chalus, K. Peterson and J.-C. Diels, Remote sensing of explosives using infrared and ultraviolet filaments, *J. Opt. Soc. Am. B*, 2008, **25**, B108.

223    B. Zeng, W. Chu, H. Gao, W. Liu, G. Li, H. Zhang, J. Yao, J. Ni, S.L. Chin and Y. Cheng, Enhancement of peak intensity in a filament core with spatiotemporally focused femtosecond laser pulses, *Phys. Rev. A*, 2011, **84**, 063819.

224    B. Zeng, T.-J. Wang, S. Hosseini, Y. Cheng, Z. Xu, W. Liu and S.L. Chin, Enhanced remote filament-induced breakdown spectroscopy with spatio-temporally chirped pulses, *J. Opt. Soc. Am. B*, 2012, **29**, 3226.

225    H.L. Xu, W. Liu and S.L. Chin, Remote time-resolved filament-induced breakdown spectroscopy of biological materials, *Opt. Lett.*, 2006, **31**, 1540.

226    H.L. Xu, G. Méjean, W. Liu, Y. Kamali, J.-F. Daigle, A. Azarm, P.T. Simard, P. Mathieu, G. Roy and J.-R. Simard, Remote detection of similar biological materials using femtosecond filament-induced breakdown spectroscopy, *Appl. Phys. B*, 2007, **87**, 151.

227    Y.-W. Zhang, X. Gao, Y. Zhang, C. Song, J.-Q. Lin, Analysis of heavy metals in poplar leaves by femtosecond filament-induced breakdown spectroscopy, *Acta Phys. Sin.*, 2015, **64**, 175203**.**

228    X. Gao, C. Du, C. Li, L Liu, C. Song, Z.-Q. Hao, J.-Q. Lin, Detection of heavy metal Cr in soil by the femtosecond filament induced breakdown spectroscopy, *Acta Phys. Sin*, 2014, **63**, 095203.

229    H.L. Xu, Y. Kamali, C. Marceau, P.T. Simard, W. Liu, J. Bernhardt, G. Méjean, P. Mathieu, G. Roy and J.-R. Simard, Simultaneous detection and identification of multigas pollutants using filament-induced nonlinear spectroscopy, *Appl. Phys. Lett.*, 2007, **90**, 101106.

230    Y. Kamali, J.-F. Daigle, F. Théberge, M. Châteauneuf, A. Azarm, Y. Chen, C. Marceau, S.C. Lessard, F. Lessard and G. Roy, Remote sensing of trace methane using mobile femtosecond laser system of T&T Lab, *Opt. Commun.*, 2009, **282**, 2062.

231    Q. Luo, H.L. Xu, S.A. Hosseini, J.-F. Daigle, F. Théberge, M. Sharifi and S.L. Chin, Remote sensing of pollutants using femtosecond laser pulse fluorescence spectroscopy, *Appl. Phys. B*, 2005, **82**, 105.

232    J.-F. Daigle, G. Méjean, W. Liu, F. Théberge, H.L. Xu, Y. Kamali, J. Bernhardt, A. Azarm, Q. Sun and P. Mathieu, Long range trace detection in aqueous aerosol using remote filament-induced breakdown spectroscopy, *Appl. Phys. B*, 2007, **87**, 749.

233    J.-F. Daigle, Y. Kamali, G. Roy and S.L. Chin, Remote filament-induced fluorescence spectroscopy from thin clouds of smoke, *Appl. Phys. B*, 2008, **93**, 759.

234    S.L. Chin, H.L. Xu, Q. Luo, F. Théberge, W. Liu, J.F. Daigle, Y. Kamali, P.T. Simard, J. Bernhardt and S.A. Hosseini, Filamentation 'remote' sensing of chemical and biological agents/pollutants using only one femtosecond laser source, *Appl. Phys. B*, 2009, **95**, 1.

235    J. Odhner and R. Levis, Optical Spectroscopy Using Gas-Phase Femtosecond Laser Filamentation, *Annu. Rev. Phys. Chem.*, 2014, **65**, 605.

236    A. De Giacomo, M. Dell'Aglio, O. De Pascale, R. Gaudiuso, A. Santagata and R. Teghil, Laser Induced Breakdown Spectroscopy methodology for the analysis of copper-based-alloys used in ancient artworks, *Spectrochim. Acta Part B*, 2008, **63**, 192.

237    S. Almaviva, R. Fantoni, L. Caneve, F. Colao, L. Fornarini, A. Santagata and R. Teghil, Use of ns and fs pulse excitation in laser-induced breakdown spectroscopy to improve its analytical performances: A case study on quaternary bronze alloys, *Spectrochim. Acta Part B*, 2014, **99**, 185.

238    M. Oujja, M. Sanz, F. Agua, J.F. Conde, M. García-Heras, A. Dávila, P. Oñate, J. Sanguino, J.R. Vázquez de Aldana, P. Moreno, M.A. Villegas and M. Castillejo, Multianalytical characterization of Late Roman glasses including nanosecond and femtosecond laser induced breakdown spectroscopy, *J. Anal. At. Spectrom.*, 2015, **30**, 1590.

239    R.K. Gill, F. Knorr, Z.J. Smith, M. Kahraman, D. Madsen, D.S. Larsen and S. Wachsmann-Hogiu, Characterization of Femtosecond Laser-Induced Breakdown Spectroscopy (fsLIBS) and Applications for Biological Samples, *Appl. Spectrosc.*, 2014, **68**, 949.

240    L. Guyon, M. Baudelet, J. Yu, J. Wolf, T. Amodeo, E. Frejafon and P. Laloi, *Laser-Induced Breakdown Spectroscopy Analysis of Bacteria: What Femtosecond Lasers Make Possible, in 15th International Conference on Ultrafast Phenomena, OSA Technical Digest Series*, 2006.

241    M. Baudelet, J. Yu, M. Bossu, J. Jovelet, J.-P. Wolf, T. Amodeo, E. Fréjafon and P. Laloi, Discrimination of microbiological samples using femtosecond laser-induced breakdown spectroscopy, *Appl. Phys. Lett.*, 2006, **89**, 163903.

242    D.C Jeong, P.S Tsai and D. Kleinfeld, Prospect for feedback guided surgery with ultra-short pulsed laser light, *Curr. Opin. Neurobiol.*, 2012, **22**, 24–33.

243    H. Huang, L.-M. Yang, S. Bai and J. Liu, Smart surgical tool, *J. Biomedical Opt.*, 2015, **20**, 028001.

244    M. Sabsabi, R. Héon and L. St-Onge, Critical evaluation of gated CCD detectors for laser-induced breakdown spectroscopy analysis, *Spectrochim. Acta Part B*, 2005, **60**, 1211.

245    P. Fichet, D. Menut, R. Brennentot, E. Vors and A. Rivoallan, Analysis by laser-induced breakdown spectroscopy of complex solids, liquids, and powders with an echelle spectrometer, *Appl. Optics*, 2003, **42**, 6029.

246    M. Sabsabi and P. Cielo, Quantitative Analysis of Aluminum Alloys by Laser-Induced Breakdown Spectroscopy and Plasma Characterization, *Appl. Spectrosc.*, 1995, **49**, 499.

247    A.A. Ilyin and S.S. Golik, Femtosecond laser-induced breakdown spectroscopy of sea water, *Spectrochim. Acta Part B*, 2013, **87**, 192.

248    P. Fichet, M. Tabarant, B. Salle and C. Gautier, Comparisons between LIBS and ICP/OES, *Anal. Bioanal. Chem.*, 2006, **385**, 338.

249    K.M. Lo and N.H. Cheung, ArF Laser-Induced Plasma Spectroscopy for Part-per-Billion Analysis of Metal Ions in Aqueous Solutions, *Appl. Spectrosc.*, 2002, **56**, 682.

250    F.-Y. Yueh, R.C. Sharma, J.P. Singh, H. Zhang and W.A. Spencer, Evaluation of the Potential of Laser-Induced Breakdown Spectroscopy for Detection of Trace Element in Liquid, *J. Air & Waste Manage. Assoc.*, 2002, **52**, 1307.

251    S.T. Järvinen, S. Saari, J. Keskinen and J. Toivonen, Detection of Ni, Pb and Zn in water using electrodynamic single-particle levitation and laser-induced breakdown spectroscopy, *Spectrochim. Acta Part B*, 2014, **99**, 9.

252    S.S. Golik, O.A. Bukin, A.A. Il'in, E.B. Sokolova, A.V. Kolesnikov, M.Y. Babiy, Y.N. Kul'chin and A.A. Gal'chenko, Determination of detection limits for elements in water by femtosecond laser-induced breakdown spectroscopy, *J. Appl. Spectrosc.*, 2012, **79**, 471.

253    J. Xiu, S. Zhong, H. Hou, Y. Lu and R. Zheng, Quantitative Determination of Manganese in Aqueous Solutions and Seawater by Laser-Induced Breakdown Spectroscopy (LIBS) Using Paper Substrates, *Appl. Spectrosc.*, 2014, **68**, 1039.

254    S.S. Golik, A.A. Ilyin, M.Y. Babiy, Y.S. Biryukova, V.V. Lisitsa and O.A. Bukin, Determination of Iron in Water Solution by Time-Resolved Femtosecond Laser-Induced Breakdown Spectroscopy, *Plasma Sci. Technol.*, 2015, **17**, 975.

255    H. Loudyi, K. Rifaï, S. Laville, F. Vidal, M. Chaker and M. Sabsabi, Improving laser-induced breakdown spectroscopy (LIBS) performance for iron and lead determination in aqueous solutions with laser-induced fluorescence (LIF), *J. Anal. At. Spectrom.*, 2009, **24**, 1421.

256    D. Santos Jr., R.E. Samad, L.C. Trevizan, A.Z. de Freitas, N.D. Vieira Jr. and F.J. Krug, Evaluation of Femtosecond Laser-Induced Breakdown Spectroscopy for Analysis of Animal Tissues, *Appl. Spectrosc.*, 2008, **62**, 1137.

257    M.D. Adamson and S.J. Rehse, Detection of trace Al in model biological tissue with laser-induced breakdown spectroscopy, *Appl. Optics*, 2007, **46**, 5844.

258    T. Owens, S.S. Mao, E.K. Canfield, C.P. Grigoropoulos, X. Mao and R.E. Russo, Ultrafast thin-film laser-induced breakdown spectroscopy of doped oxides, *Appl. Optics*, 2010, **49**, C67.

259    J. Xiu, V. Motto-Ros, G. Panczer, R. Zheng and J. Yu, Feasibility of wear metal analysis in oils with parts per million and sub-parts per million sensitivities using laser-induced breakdown spectroscopy of thin oil layer on metallic target, *Spectrochim. Acta Part B*, 2014, **91**, 24.

260    G.G. Arantes de Carvalho, J. Moros, D. Santos Jr., F.J. Krug and J.J. Laserna, Direct determination of the nutrient profile in plant materials by femtosecond laser-induced breakdown spectroscopy, *Anal. Chim. Acta*, 2015, **876**, 26.

261    Ş. Yalçın, S. Örer and R. Turan, 2-D analysis of Ge implanted $SiO_2$ surfaces by laser-induced breakdown spectroscopy, *Spectrochim. Acta Part B*, 2008, **63**, 1130.

262    I. Lopez-Quintas, V. Pinon, M.P. Mateo and G. Nicolas, Effect of surface topography in the generation of chemical maps by laser-induced plasma spectroscopy, *Appl. Surf. Sci.*, 2012, **258**, 9432.

263    Y. Markushin, P. Sivakumar, D. Connolly and N. Melikechi, Tag-femtosecond laser-induced breakdown spectroscopy for the sensitive detection of cancer antigen 125 in blood plasma, *Anal. Bioanal. Chem.*, 2015, **407**, 1849.